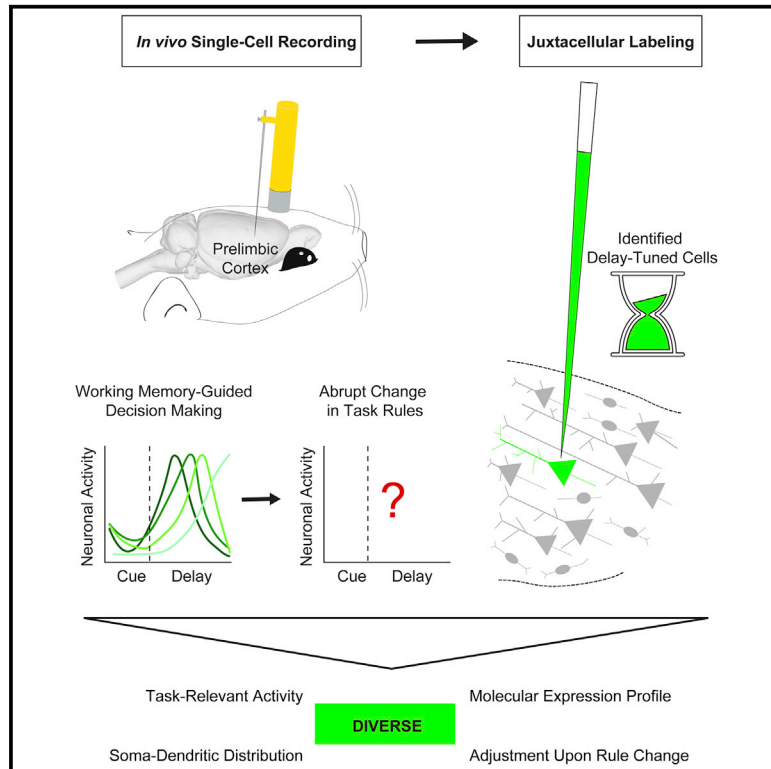


Unexpected Rule-Changes in a Working Memory Task Shape the Firing of Histologically Identified Delay-Tuned Neurons in the Prefrontal Cortex

Graphical Abstract



Authors

A. Tugrul Ozdemir, Michael Lagler, Sabria Lagoun, Hugo Malagon-Vina, Balint Lasztóczy, Thomas Klausberger

Correspondence

tugrul.ozdemir@pharm.ox.ac.uk (A.T.O.), thomas.klausberger@meduniwien.ac.at (T.K.)

In Brief

Ozdemir et al. perform juxtacellular recording and labeling of delay-tuned neurons in rats performing a working memory task. They show that these cells are heterogeneous in molecular expression and somato-dendritic organization. Unexpected change of the task rule diversely adjusts firing activity of the delay-tuned neurons and prefrontal networks.

Highlights

- Juxtacellular recording and labeling of neurons during a working memory task
- Molecular and somato-dendritic heterogeneity of delay-tuned neurons
- Unexpected change of the task rule diversely adjusts activity of delay-tuned neurons
- Cognitive flexibility induces changes in prefrontal networks and delay-tuned neurons



Unexpected Rule-Changes in a Working Memory Task Shape the Firing of Histologically Identified Delay-Tuned Neurons in the Prefrontal Cortex

A. Tugrul Ozdemir,^{1,2,*} Michael Lagler,¹ Sabria Lagoun,¹ Hugo Malagon-Vina,¹ Balint Lasztóczy,¹ and Thomas Klausberger^{1,3,*}

¹Center for Brain Research, Division of Cognitive Neurobiology, Medical University of Vienna, Vienna 1090, Austria

²Present address: Department of Pharmacology, University of Oxford, Oxford OX1 3QT, UK

³Lead Contact

*Correspondence: tugrul.ozdemir@pharm.ox.ac.uk (A.T.O.), thomas.klausberger@meduniwien.ac.at (T.K.)

<https://doi.org/10.1016/j.celrep.2019.12.102>

SUMMARY

Working memory-guided behaviors require memory retention during delay periods, when subsets of prefrontal neurons have been reported to exhibit persistently elevated firing. What happens to delay activity when information stored in working memory is no longer relevant for guiding behavior? In this study, we perform juxtacellular recording and labeling of delay-tuned (-elevated or -suppressed) neurons in the prelimbic cortex of freely moving rats, performing a familiar delayed cue-matching-to-place task. Unexpectedly, novel task-rules are introduced, rendering information held in working memory irrelevant. Following successful strategy switching within one session, delay-tuned neurons are filled with neurobiotin for histological analysis. Delay-elevated neurons include pyramidal cells with large heterogeneity of soma-dendritic distribution, molecular expression profiles, and task-relevant activity. Rule change induces heterogenous adjustments on individual neurons and ensembles' activity but cumulates in balanced firing rate reorganizations across cortical layers. Our results demonstrate divergent cellular and network dynamics when an abrupt change in task rules interferes with working memory.

INTRODUCTION

The prefrontal cortex is involved in the executive functioning of the brain (Fuster, 2015; Miller and Cohen, 2001). It has been suggested to orchestrate thought and action in working memory-guided decision-making and conflict monitoring in goal-directed behavior (Miller and Cohen, 2001). Working memory refers to the ability to temporarily retain and manipulate information over a course of seconds (Baddeley, 1992). Early electrophysiological recordings in nonhuman primates revealed single prefrontal neurons with sustained spiking activity during the delay period of the working memory tasks (Fuster and Alexander, 1971; Kojima and

Goldman-Rakic, 1982; Kubota and Niki, 1971). Since the buffering of information in a brief active state is a hallmark of working memory, persistent delay activity appeared as a neuronal blueprint of working memory in the literature (Funahashi et al., 1993). Consistent with this notion, lesions in the dorsolateral prefrontal cortex in primates impede the performance in delayed-response tasks with increasing severity as the length of the delay period is extended (Bauer and Fuster, 1976; Funahashi et al., 1993; Jacobsen, 1936). In rodents, delay-restricted optogenetic perturbation of the medial prefrontal cortex is sufficient to diminish the working memory-guided behavior (Kamigaki and Dan, 2017; Bolkan et al., 2017; Rossi et al., 2012; Liu et al., 2014). However, the cue-outcome contingencies bridged by working memory are not fixed. Due to everlasting changes we encounter in our daily lives, we must monitor the outcome of our actions and flexibly adjust future strategies and the relevance attributed to the items stored in the working memory. If the current strategy for working memory is no longer useful, would the persistent delay activity be disrupted?

As is for the working memory, the control of flexible behavior to assess and update strategies is dependent on an intact prefrontal cortex in humans (Milner, 1963; Szczepanski and Knight, 2014), monkeys (Buckley et al., 2009; Dias et al., 1996), and rodents (Joel et al., 1997; Rich and Shapiro, 2009; Ragozzino et al., 1999). In light of previous actions resulting in a negative or positive outcome, one should be able to adjust the behavior flexibly. Adjustment of behavior requires disengaging from a previous task, reconfiguring a new set of responses, and implementation to maximize the positive outcome. Cognitive flexibility broadly refers to the mental ability to adapt thoughts and action plans in rapidly changing environments. In rodents, this has been studied in diverse contexts of processes such as task strategy switching (Malagon-Vina et al., 2018; Rich and Shapiro, 2009; Ragozzino et al., 1999), attentional set-shifting (Birrell and Brown, 2000; Durstewitz et al., 2010; Del Arco et al., 2017; Rikhie et al., 2018), or reversal learning (Murray et al., 2015; Matias et al., 2017; Nakayama et al., 2018). Nevertheless, the link between working memory and cognitive flexibility, and how single prefrontal neurons contribute to these two behaviors dynamically, remains largely unknown.

The cerebral cortex consists of distinct types of neuron that orchestrate network activity differentially. Dissecting the network



into its building blocks and characterizing the functional role of each cell is critically important for understanding the sum. With the advances in viral and transgenic technologies in mice, recent studies showed that prefrontal pyramidal neurons with diverse projection routes and molecular expression profiles contribute differently to task-relevant processes (Kim et al., 2017; Murugan et al., 2017; Nakayama et al., 2018). The activity of single prefrontal neurons can reflect various combinations of behaviorally relevant aspects of working memory tasks, providing a high degree of functional heterogeneity and complexity (Euston et al., 2012; Miller, 2013; Rigotti et al., 2013). Prominently, the persistent delay activity of a subset of prefrontal neurons can predict trial outcome (Hardung et al., 2017; Lagler et al., 2016; Fujisawa et al., 2008; Narayanan and Laubach, 2006; Kamigaki and Dan, 2017), and not merely choice expectancy (Del Arco et al., 2017), movement (Schmitt et al., 2017; Lindsay et al., 2018) or location (Lindsay et al., 2018). Delay activity might be central to working memory, but its role in adaptive behavior remains undiscovered. Neither the identity of the delay-tuned (-elevated or -suppressed) neurons nor their role in adaptive behavior has been revealed. In this study, we used a combination of extracellular multiple single-unit recordings and targeted single-neuron recording of identified cells in rats performing a delayed cue-matching-to-place task followed by an unexpected rule change rendering the cue irrelevant in informing behavior. Our results demonstrate the diversity among labeled delay-tuned cells in the medial prefrontal cortex as well as their differential activity adjustments during the rule changing/re-learning.

RESULTS

Working Memory-Guided Decision-Making Task Followed by an Abrupt Rule Change

We trained 16 rats to perform a delayed cue-matching-to-place task on an elevated Y maze. In this task, rats associated a randomly given cue (chocolate- or cherry-flavored water) with a specific location (left or right arm, respectively) to receive a reward (Figure 1A, left). To probe working memory, at the end of the cue delivery rats had to wait behind a moveable door for 6 s before going to one of the two reward arms (Fujisawa et al., 2008). In error trials, the rats did not receive any reward and thus had to return to the start arm to initiate the next trial (Figure 1B). We previously confirmed that prelimbic cortex activity is necessary for a correct performance in this delayed cue-matching-to-place task paradigm (Lagler et al., 2016) (referred to as rule 1 henceforth). When the animals reached 75% accuracy in task performance (average correct performance $89.7\% \pm 6.9\%$) during rule 1, we introduced an abrupt rule change after which rats could receive the reward only in one of two reward locations regardless of the cue type (hereafter called rule 2; Figure 1A, right). While animals were well trained for rule 1, they encountered rule 2 unexpectedly and only during recording sessions. After the rule change, while one of the cue-reward contingencies remained stable, the other one led to the conflicting trials. As expected, this change led to reduced success in conflicting trials during which the rats started to make a number of errors by following the previous rule (referred to as rule 2-naive henceforth). When the rats switched the behavioral strategy in

five consecutive conflicting trials, excluding the intermixed non-conflicting trials, we called this period rule 2-learned, since the rats had started to achieve evidence-based rule learning (Figure 1C). All rats included in this study managed to learn the new rule in a single behavioral session (Figure 1D). While there was no spatial preference for the reward arms during rule 1, expectedly the number of errors was significantly greater in conflicting trials than in non-conflicting trials (Figure 1E).

Prefrontal Neurons Exhibit Sustained but Diversely Tuned Task-Episode Modulation during Rule Changing/ Re-learning

We performed extracellular recordings from single cells in the medial prefrontal cortex (mPFC) of behaving rats using tetrodes, glass electrodes, or silicon probes across all cortical layers. Activity in the mPFC is crucial for the flexible cognitive control (Nakayama et al., 2018). How do single prefrontal neurons contribute to the flexible cognitive control when the well-trained subjects encounter a conflict in task rules abruptly? At the single-cell level, we observed that simultaneously recorded mPFC units can undergo opposite changes in firing activity upon the learning of the new task rule during different epochs (Figure 2A). It has been reported that single prefrontal neurons exhibit diverse mixtures of responsivity upon switching contexts, yet the reallocations are tightly balanced across neuronal populations (Ma et al., 2016). Consistently, we found that the overall firing rate across rule 1, rule 2-naive and rule 2-learned remained unchanged at the population level ($p = 0.7470$, Friedman's test, *post hoc* Dunn's multiple comparisons test). To capture overall significant changes in firing rate, we calculated a rule change score (RCS) across rule 1 to rule 2-learned (see STAR Methods for details). The fraction of the units eliciting a significant increase in firing activity (28% of all recorded units) was comparable to the proportion of the units that reduced their firing activity (31% of all recorded units) as calculated by overall $RCS_{\text{Rule1,learned}}$ (Figure 2B). Notably, these adaptations in firing rate were independent of the laminar position of the recorded cell bodies, suggesting well-distributed and -balanced reorganization of the firing rate in the mPFC rather than an overall network excitation or inhibition during learning of the new task rule (Figure 2C).

Consistent with previous reports (Lagler et al., 2016; Fujisawa et al., 2008), we observed prefrontal units to be highly task episode modulated, tiling their maximal firing activity along the sequential task episodes on the maze during the working memory paradigm (rule 1), possibly raising a division of labor in the local network (Figure 2D, left). Interestingly, neither the onset of the rule change nor the learning of the new task rule immensely affected the task-episode modulation of the single cells in the mPFC (Figure 2D, middle and right). 70 out of 123 units retained similar firing rate fluctuations across different task epochs during the learning the new task (Figure 2E). Because many cells kept their relative firing patterns, there was a high correlation between the neuronal activity of the cells during the matching episodes of rule 1 and rule 2-learned at the population level (Figure 2F). We sought to understand in which task episodes the firing activity of cells undergoes the greatest changes with the learning of the new task rule. Comparing the correlation coefficients calculated from the transition between rule 1 and rule 2-naive and rule

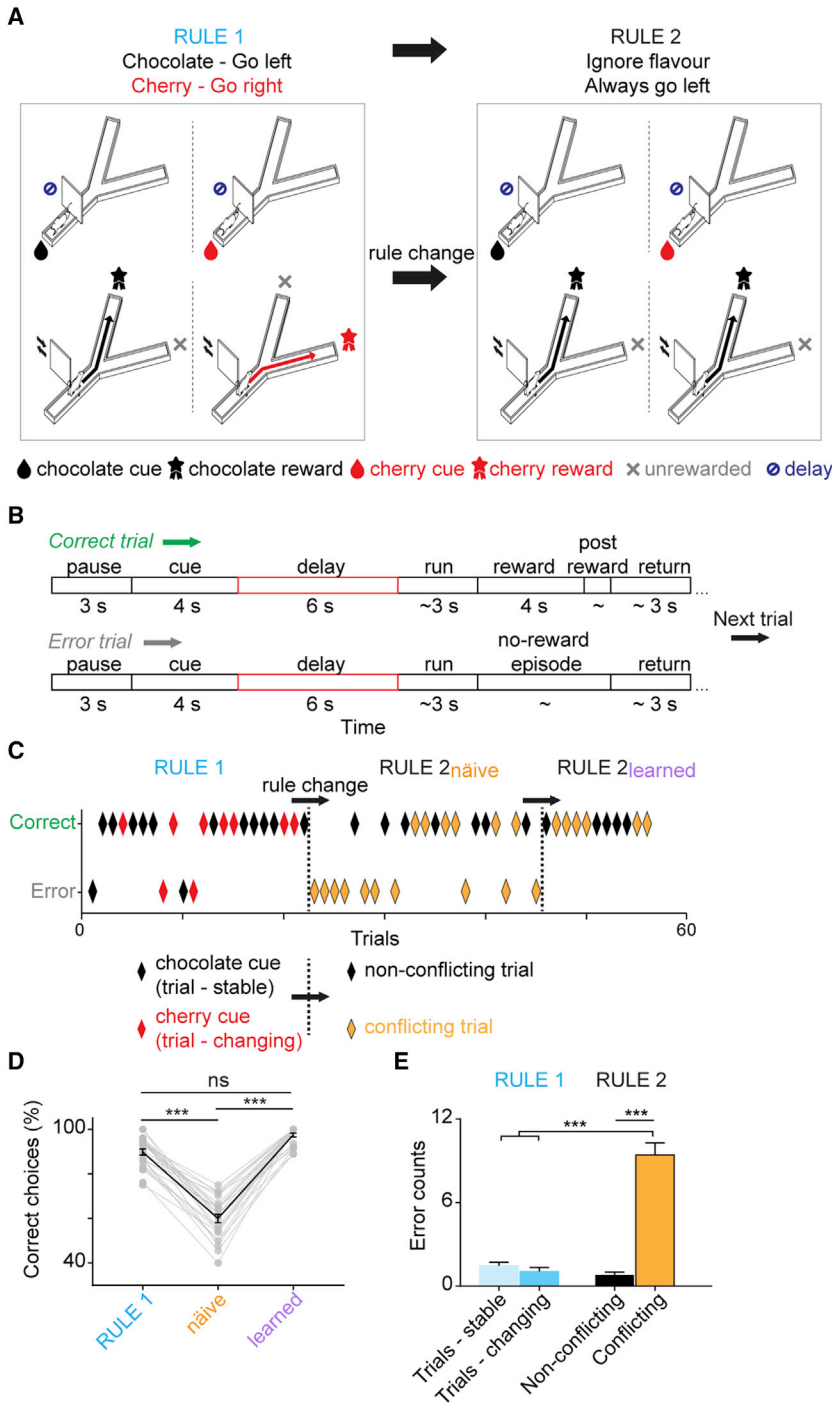


Figure 1. A Delayed Cue-Matching-to-Place Task Followed by an Abrupt Rule Change

(A) Schematic of the behavioral task. Left: rats were well trained to associate a randomly given cue (chocolate- or cherry-flavored water) with a reward location (left or right, respectively) on an elevated Y maze (rule 1). At the end of cue delivery, rats had to wait for 6 s (delay) in the start arm before executing their choice. Right: upon correct task performance during rule 1, a rule change was introduced; thereafter, the rats could receive the reward only in one of the reward locations regardless of the cue type (rule 2). While the rats were well trained for rule 1, they unexpectedly encountered rule 2 during a recording session.

(B) Description of the sequential task episodes in correct and error trials.

(C) Task performance of a rat in one behavioral session. Each mark indicates a trial (black, chocolate trials; red, cherry trials). Upon rule change (rule 2-naïve), the rat started to make several errors as it was following the previous rule. If the rat successfully switched the strategy in five consecutive conflicting trials (orange with black border) (excluding the non-conflicting trials), behavioral criterion was reached for learning (rule 2-learned).

(D) Task performance dropped upon rule change across the behavioral sessions and all animals could reach the criterion for learning (N = 24 sessions; $p = 2.6471e-11$, Friedman's test, *post hoc* Dunn's multiple comparisons test). Gray lines, individual sessions; black, mean \pm SEM. *** $p < 0.0001$.

(E) Task performance was balanced among the different trial types of rule 1, whereas naïve errors arose from the conflicting trials during rule 2, where one of the cue types no longer matches with the previously associated reward location (N = 24 sessions; $p = 2.6895e-12$, Kruskal Wallis test, *post hoc* Dunn's multiple comparisons test). Error bars denote SEM. *** $p < 0.0001$.

1 and rule 2-learned, we found the elevated firing during periods of pause (immobile intertrial interval), delay, run (forward run), and return (back run) significantly changed upon learning (Figure 2G). Collectively, prefrontal units kept their relative firing patterns on the maze but diversely tuned their activity during cognitive flexibility.

Cell assemblies formed by strongly interconnected groups of co-active neurons are thought to represent distinct cognitive

entities (Hebb, 1949; Buzsáki, 2010). As described in van de Ven et al. (2016), we aimed to identify groups of mPFC cells with repeated coincident firing activity within 25-ms time windows. Simultaneously recorded cells from 3 sessions (N = 94 cells) formed a total of 12 patterns (4 ± 1) during delayed cue-matching-to-place task (rule 1). Five assembly patterns from one of the recording sessions are shown in Figure S1Ai. We observed that some of these detected assemblies grouped together units with similar episodic firing patterns during the working memory task, tiling the neural activity along the Y maze (Figure S1Aii). Cell assemblies can be detected outside the task context, yet often reinstated when engaged in the task (Trouche et al., 2019). Seven of 12 detected cell assemblies had significantly higher expression strengths during task epochs compared to the immobile intertrial interval across trials during rule 1 ($p < 0.05$ in pairs, Wilcoxon matched-paired signed rank test),

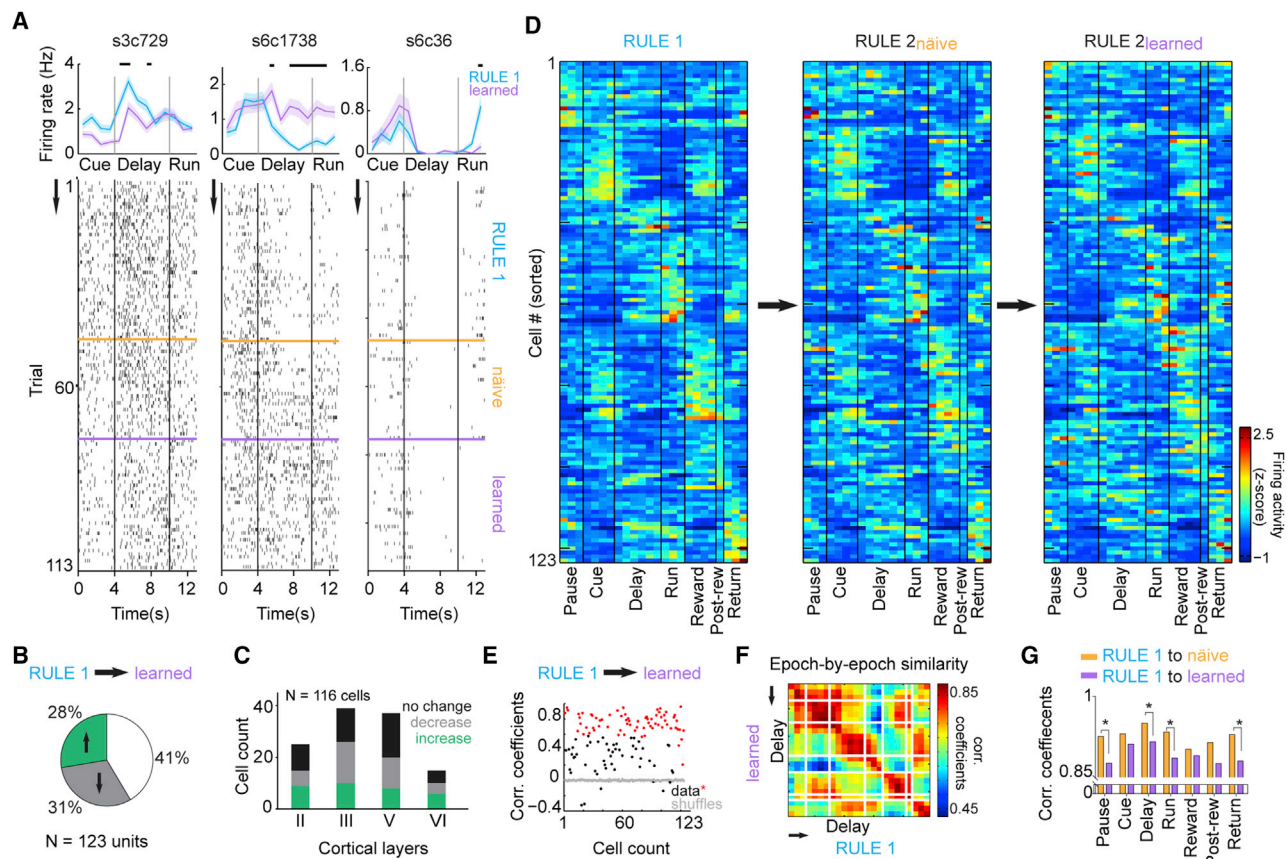


Figure 2. Neurons in the mPFC Exhibit Sustained but Diversely Scaled Task-Episode Modulation during Cognitive Flexibility

(A) Top: three simultaneously recorded units that show significant discrimination across rule 1 and rule 2-learned in diverse epochs. Horizontal bars indicate significant differences in firing rate ($N_{rule1} = 46$, $N_{learned} = 38$; $p < 0.0001$, $F(12,1066) = 11.74$, $F(12,1066) = 7.002$, $F(12,1066) = 11.93$ [left, middle, and right unit, respectively] two-way ANOVA, *post hoc* Sidak's multiple comparisons test). Dark lines, mean firing rate; shading, mean \pm SEM. Bottom: raster plots of the corresponding units, showing trial-by-trial firing activity during the behavioral task.

(B) Percentage of the units that exhibited increased, decreased, or stable firing activity upon learning the new task rule as calculated by rule change scores (RCSs) (see STAR Methods for details).

(C) Laminar positions of 116 units (of all 123 recorded units) in the cortex could be determined. Cells showing increased, decreased, or stable firing activity were heterogeneously distributed across cortical layers ($p = 0.6225$, Chi-square test).

(D) Firing activity of the mPFC cells was tiled along different epochs of the behavioral task (left) even after the rules were changed (middle and right). Each cell's firing pattern is normalized (Z score) individually across rule 1, rule 2-naïve and rule 2-learned on all correct trials, averaged, and sorted based on the time when their maximal firing activity occurred during rule 1. Color bar indicates the normalized firing activity.

(E) Spearman's rank correlation coefficient between rule 1 and rule 2-learned was calculated on each cell (black, data; red, data denoting significant correlations after Bonferonni-Holm correction for multiple comparison; gray, mean correlation coefficient from the shuffled dataset, 1,000 repetitions). 56.9% of the cells (70 out of 123) exhibited a sustained firing pattern.

(F) Pairwise Spearman's rank correlation matrix across rule 1 and rule 2-learned showed sustained firing patterns in sequential task epochs. Color bar denotes correlation coefficients.

(G) Fisher's z transformation on the correlation coefficients obtained from rule 1 to rule 2-naïve and from rule 1 to rule 2-learned. Asterisks denote significance on sequential task epochs across learning ($N_{r-values} = 123$, $P_{pause} = 0.026$, $P_{cue} = 0.3295$, $P_{delay} = 0.0326$, $P_{run} = 0.0274$, $P_{reward} = 0.6186$, $P_{post-reward} = 0.1232$, $P_{return} = 0.0324$).

See also Figure S1

although the direct causal relevance of the detected mPFC cell assemblies to the task performance has not been examined in this study. Next, we sought to investigate whether the detected assemblies would undergo alterations with a change in task rule, for which, we quantified the expression strength of the detected assemblies and tracked the changes in strength on a trial-by-trial basis across the entire recording session (Figure S1Aiii). We

found 58.3% (7 out of 12) of the detected cell assemblies during rule 1 underwent significant changes in expression strength during rule 2 (Figure S1B). Yet, when we exclusively used the spike times during rule 2 only, 83.7% (10 out of 12) of the detected cell assembly patterns matched with the assembly patterns during rule 1 (Figure S1C). Interestingly, we observed two additional patterns forming after the rule change, suggestive of the

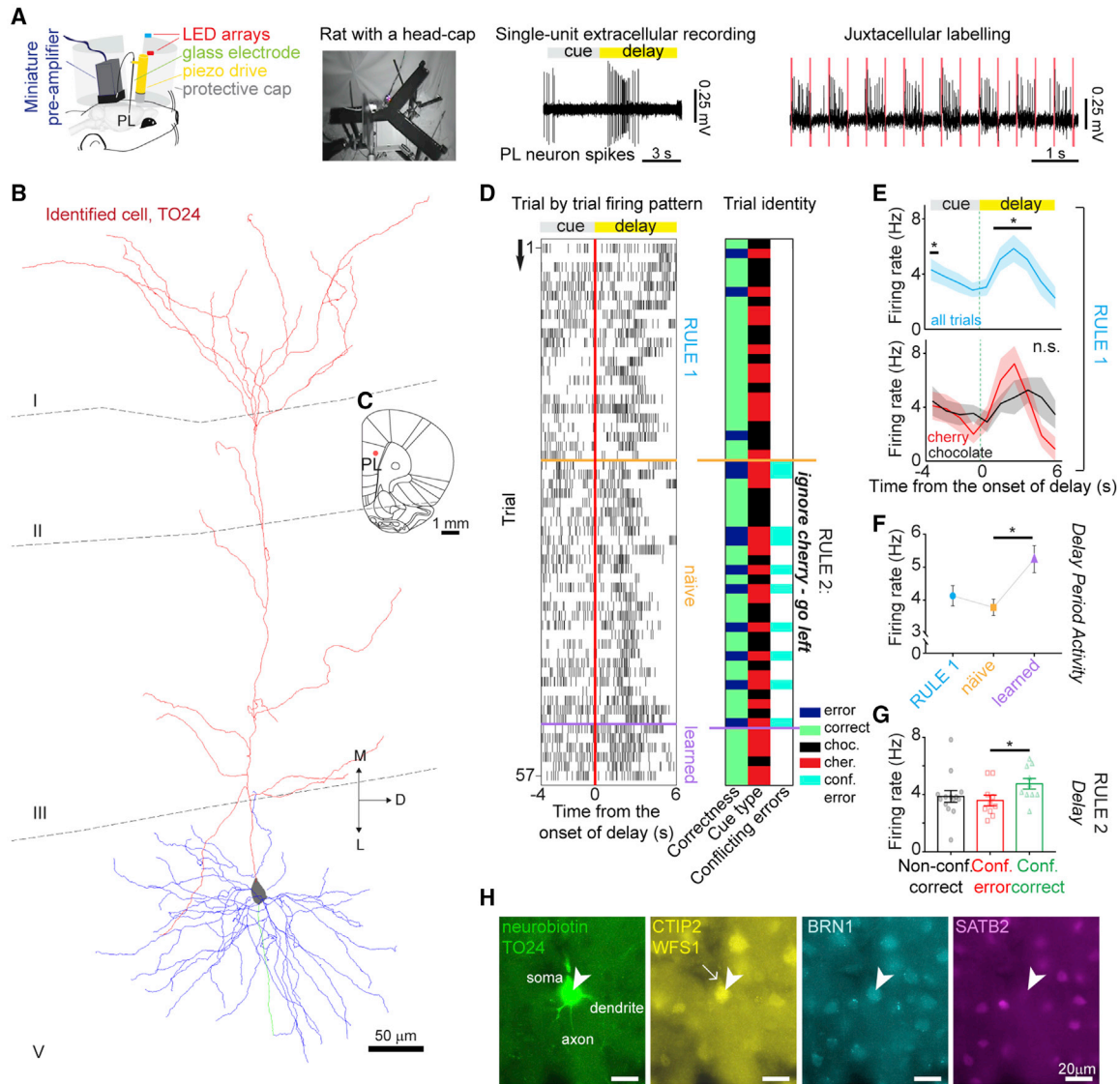


Figure 3. Juxtacellularly Recorded and Labeled Layer V Neuron in the Prelimbic Cortex with Elevated Spiking Activity during the Delay Period of the Working Memory Task and Its Distinct Rate Adaptation during Cognitive Flexibility

(A) Action potentials of single prelimbic neurons were recorded extracellularly using glass electrodes in rats during consecutive working memory and cognitive flexibility tasks. Delay-tuned cells preselected based on their elevated or decreased neuronal activity from cue to delay epochs were then juxtacellularly labeled with neurobiotin.

(B) Reconstruction of the identified delay-elevated pyramidal neuron, TO24, located in the layer V of the prelimbic cortex (blue, basal dendrites; red, apical dendrite; green, main axon) (thickness: 50 μ m, 7 coronal sections).

(C) Position of the labeled cell body (shown with a red dot) in the tissue section (D, dorsal; L, lateral; M, medial).

(D) Left: raster plot of the delay-elevated cell, TO24, across all trials during working memory and cognitive flexibility. Right: trial identifier showing trial-by-trial accuracy (blue, error; green, correct) and cue type (black, chocolate; red, cherry), as well as conflicting trials ending with a negative outcome (turquoise, conflicting error).

(E) Top: cell TO24 showed ramping neuronal activity during the delay period of the working memory task (rule 1). Horizontal bars with asterisks indicate significance in firing rate change (*adjusted $\alpha = 0.011$, significance thresholds were calculated using a shuffling procedure on all correct trials and alpha values were corrected by the false discovery rate [FDR] method; see STAR Methods for details). Bottom: persistent firing activity during the delay is not stimulus specific (cherry versus chocolate trials) during the working memory paradigm (rule 1) ($N_{chocolate} = 11$, $N_{cherry} = 9$ trials; n.s., permutation test on all correct trials with two conditions; FDR correction; see STAR Methods for details). Dark lines, mean firing rate; shade, mean \pm SEM.

(F) Delay-elevated neuron, TO24, showed significant increase in firing rate upon learning the new task rule (rule 2-learned) ($N_{Rule1} = 23$, $N_{naive} = 28$, and $N_{learned} = 6$ trials; $p = 0.0175$, Kruskal-Wallis test, *post hoc* Dunn's multiple comparisons test). Error bars denote \pm SEM. * $p < 0.05$.

(legend continued on next page)

possibility that new prefrontal cell assemblies can be formed during cognitive flexibility.

Individual Delay-Tuned Cells Exhibit Diverse Firing Pattern Adjustments and Alter Non-uniformly upon a Rule Change

Having shown mPFC neurons and ensembles with sequential and episode-specific firing activity throughout the behavioral paradigm, we decided to focus on the delay period, which is critically discussed if it might be central to the working memory. We aimed to identify delay-tuned (elevated or suppressed) neurons from rats engaged in a working memory task and investigate their firing dynamics upon an unexpected change in task rules. The unequivocal identification of the delay-tuned neurons was achieved by online monitoring of the single neurons' persistent ramping or dampening spiking activity during the delay period of the working memory task (rule 1) and by subsequent juxtacellular labeling to aid their further characterization and anatomical analyses (Figure 3A; Video S1). Each rat was trained on rule 1 for approximately 2 h/day for ~8 weeks. Only one neuron was labeled per animal that had >75% in task performance during rule 1 and managed to reach the set behavioral criterion for the learning upon a rule change within the same recording session.

We sought to investigate the shared and divergent properties that delay-tuned cells might possess (Figures 3, 4, 5, and S2). Dendritic reconstruction of two *in vivo* recorded and juxtacellularly labeled delay-elevated cells in serial sections revealed distinct dendritic trees such as the presence of a prominent thick apical dendrite with a broad and extensive bifurcation in the layer I of the prelimbic cortex (PL) (Figures 3B and 4A). The position of the labeled delay-elevated cell bodies (N = 6) was spread along the anteroposterior and mediolateral axes in the PL, not exhibiting similar laminar localization (Figures 3C, 4B, and 5A), and the delay-tuned cells exhibited diverse autocorrelation histograms (Figure 5B). Consistent with a recent report on mice performing a spatial working memory task (Bolkan et al., 2017), the peak of delay spiking activity in individual cells was distributed over the time span of the delay, with each neuron showing a preferred temporal offset within the delay period (Figures 3D and 3E, top; Figures 4C and 4D, top; and Figures 5C and 5E). The firing pattern of the delay-elevated cells in the mPFC has been shown to correlate with certain task rules in working memory-guided behavioral paradigms in mice (Schmitt et al., 2017; Bolkan et al., 2017). We asked whether the activity of our identified cells differed depending on the upcoming choice during rule 1 (Figure 3E, bottom; Figure 4D, bottom; and Figure 5E). We observed that two labeled delay-elevated neurons (layer V pyramidal neuron, TO20; layer II pyramidal neuron TO36) exhibiting a differential firing activity between correct cherry (right choices) and

chocolate trials (left choices) during at least 1 s of the delay period but not during stimulus presentation, which are often deemed as “choice-selective cells” in the literature (Figure 5E). One labeled cell (TO34) also showed differential firing activity during stimulus sampling (cue), which may not explicitly reflect choice selectivity but may also involve perhaps a sensory response to stimuli (Figure 4D, bottom). Overall, we did not observe a systematic pattern for choice selectivity among the labeled delay-elevated cells during rule 1. It is important to note that in behavioral paradigms with only two choices, differentiating between cue and choice selectivity is restricted with the experimenters' limited interpretation.

What happens to the elevated spiking activity during the delay period when encountering a conflict of rules? Confirming our earlier results from the population analyses (Figure 2), we did not observe a trend of change in firing activity (overall increase or decrease) of the labeled delay-elevated cells during rule 2 (Figures 3F, 4E, and 5D). While one identified delay-elevated cell (TO24) increased its firing activity upon learning the new task rule (rule 2-learned) (Figures 3F and 5D), another delay-elevated cell (TO34) decreased its firing activity with the progression of the task upon rule change (Figures 4E and 5D). Because the conflict caused by the rule change reshapes the well-learned behavior, we next sought to investigate whether the neuronal activity during the delay period in these cells would reflect a potentially adapted strategy in conflicting trials after the rule change (rule 2). Interestingly, we observed differences in the firing rate of the identified cell TO24 during the delay period when the animal followed the old rule or applied the new rule in the conflicting trials (Figure 3G). However, this was not observed among the other identified delay-tuned units (Figures 4F and 5F). Two identified cells' (TO15's and TO34's) conditional firing rates varied among the conflicting and non-conflicting trials, reminiscent of their differential activity among correct left and right choices during the working memory paradigm (rule 1).

The cerebral cortex comprises a variety of specialized cell types and the contribution of these cell types to behavior remains largely unknown. Expression of specific genes can define subtypes of pyramidal neuron populations in the cerebral cortex (Molnár and Cheung, 2006; Lodato and Arlotta, 2015; Kim et al., 2017; Nakayama et al., 2018). We first aimed to profile the immunohistochemical expression pattern of the pyramidal neurons in the rat prelimbic cortex using available markers (Figures S2, 3H, and 4G; Table 1). Then we sought to answer whether the delay-elevated neurons represent a distinct cell type according to their molecular expression profiles. We tested labeled delay-elevated cells' immunoreactivity for three transcription factors—CTIP2 (BCL11B), SATB2, and BRN1—and a transmembrane protein WFS1. All tested cells were immunopositive for CTIP2; however,

(G) Delay firing activity during rule 2 was distinct in trials when the rat followed the old strategy of rule 1 (red, conflicting error) compared to when the animal switched the strategy according to rule 2 (green, conflicting correct). $N_{non-conf. correct} = 14$, $N_{conf. error} = 10$, and $N_{conf. correct} = 10$ trials; $p = 0.0335$, Kruskal-Wallis test, *post hoc* Dunn's multiple comparisons test. Error bars denote \pm SEM. * $p < 0.05$

(H) Neurobiotin-labeled delay-elevated cell TO24 (green, soma) was CTIP2⁺ (arrowhead, nucleus; yellow), WFS1⁺ (arrow, peri nuclear; yellow), BRN1⁺ (arrowhead, nucleus; cyan), and SATB2⁻ (arrowhead, nucleus; magenta). Note, WFS-1 immunoreactivity was tested following the detection of Ctip2 expression in a series of reactions.

See also Figure S2 and Table 1

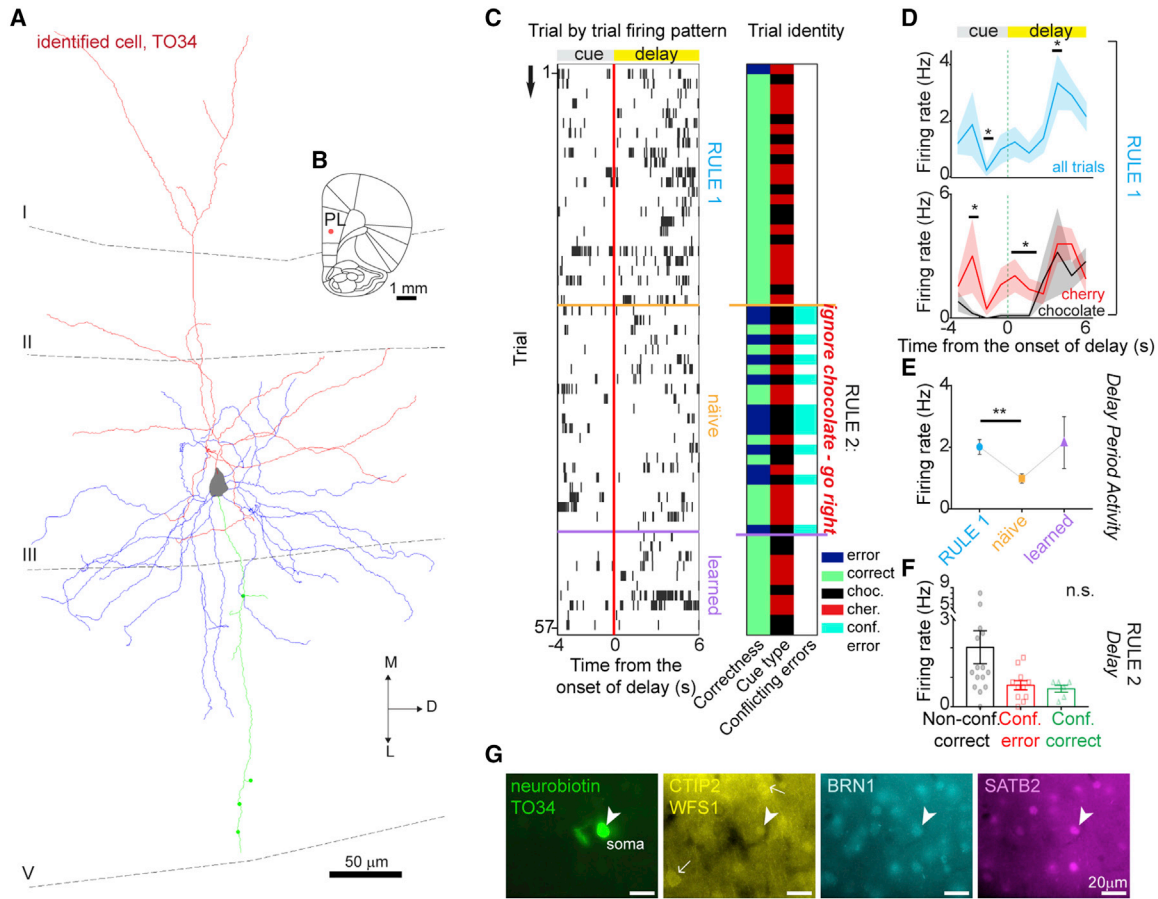


Figure 4. Identified Layer III Neuron Exhibiting Elevated Spiking Activity during the Delay Period of the Working Memory Task and Its Distinct Rate Adaptation during Cognitive Flexibility

(A) Reconstruction of the identified delay-elevated pyramidal neuron, TO34, located in layer III of the prelimbic cortex (section thickness: 50 μ m, 5 sections) (blue, basal dendrites; red, apical dendrite; and green, main axon). Red dot indicates the position of the cell body (D, dorsal; M, medial; and L, lateral).

(B) Position of the labeled cell body (shown with a red dot) in the tissue section (D, dorsal; L, lateral; M, medial).

(C) Left: raster plot of the delay-elevated cell, TO34, across all trials during working memory and cognitive flexibility. Right: trial identifier as in Figure 3D.

(D) Identified cell, TO34, showed ramping neuronal activity during the delay period of the working memory task (rule 1). Horizontal bars with asterisks indicate significance in firing rate change (*adjusted $\alpha = 0.0096$, significance thresholds were calculated using a shuffling procedure on all correct trials; FDR for multiple comparison; see STAR Methods for details). Bottom: firing activity during delay is stimulus specific (chocolate versus cherry trials) during the working memory paradigm (rule 1) ($N_{chocolate} = 9$, $N_{cherry} = 14$ trials; *adjusted $\alpha = 0.0093$, permutation test on all correct trials with two conditions; FDR correction; see STAR Methods for details). Dark lines, mean firing rate; shading, mean \pm SEM.

(E) Delay-elevated cell, TO34, exhibited significant decrease in firing rate upon rule change ($N_{rule\ 1} = 24$, $N_{naive} = 23$, and $N_{learned} = 10$ trials; $p = 0.0126$, Kruskal-Wallis test, *post hoc* Dunn's multiple comparisons test). Error bars denote \pm SEM. ** $p < 0.01$.

(F) Delay firing activity of cell TO34 during rule 2 across correct non-conflicting trials, and correct or incorrect conflicting trials ($N_{non-conf. correct} = 15$, $N_{conf. error} = 11$, and $N_{conf. correct} = 6$ trials; $p = 0.0337$, Kruskal-Wallis test, n.s. in *post hoc* Dunn's multiple comparisons test). Error bars denote \pm SEM.

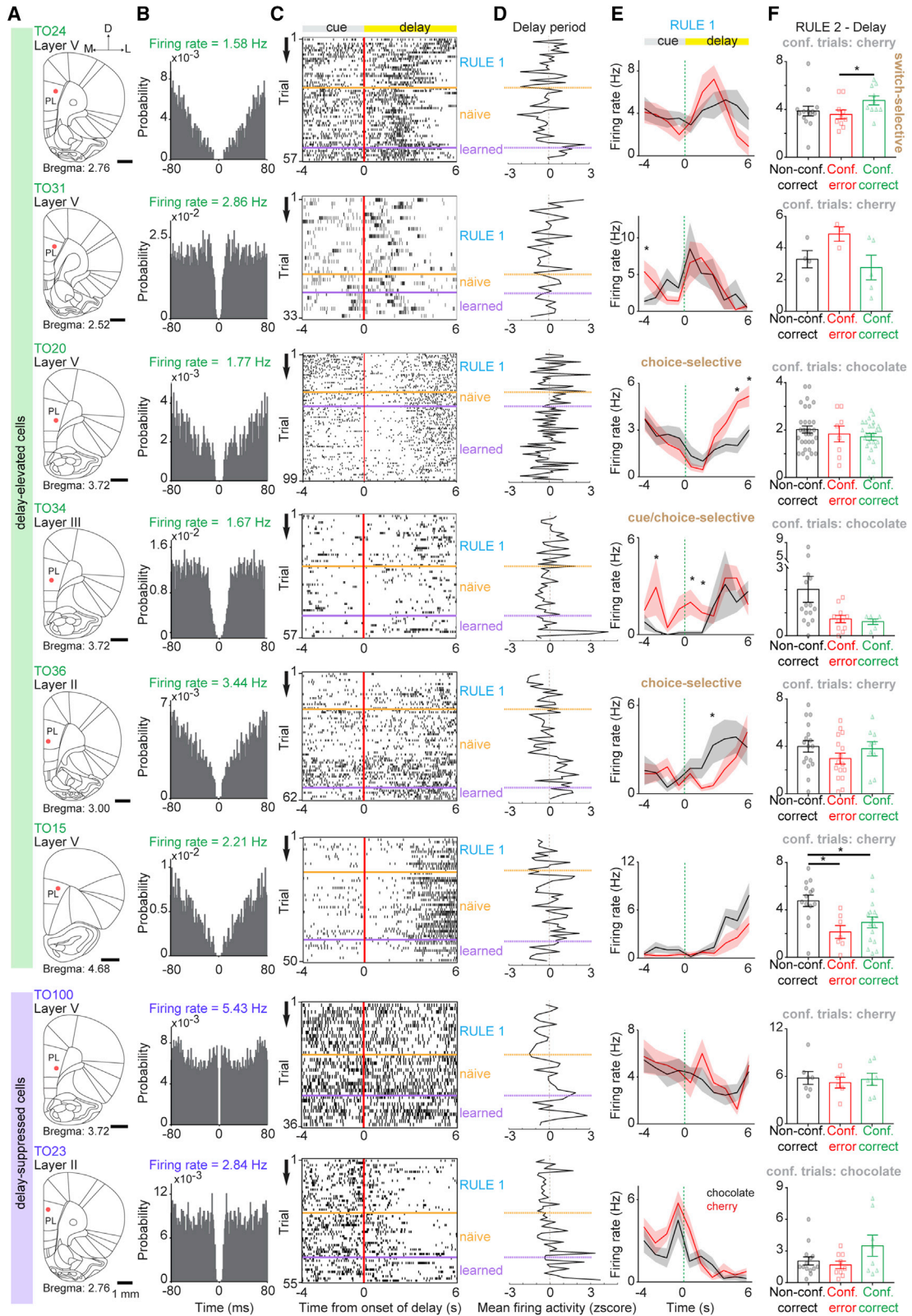
(G) Neurobiotin-labeled delay-elevated cell, TO34 (green, soma), was BRN1⁺ (arrowhead, nucleus; cyan), SATB2⁺ (arrowhead, nucleus; magenta), and CTIP2⁺ (arrowhead, nucleus; yellow) but lacked detectable immunoreactivity for WFS-1 (arrow, peri nuclear; yellow).

See also Figure S2 and Table 1

we observed diverse combinations of expression for the other tested markers across labeled cells ($N = 5$) (Figures 3H and 4G; Table 1).

We also observed a larger group of units ($N = 45$ out of 123 units) exhibiting significantly less neuronal activity during the delay period, gradually reducing its spiking frequency from stimulus sampling to the delay, contrary to delay-elevated neurons. Here, we report two identified delay-suppressed cells (TO100 and TO23), recorded from layer V and layer II of the prelimbic

cortex during the cognitive task. These two identified pyramidal neurons' activity did not reflect accuracy, cue/choice selectivity, or updated strategy (Figures 5D–5F), and all tested immunopositive for CTIP2, SATB2, BRN1, and WFS1 (Table 1). Similar to the delay-elevated cells' diverse rate adjustment with conflict in the task rules, cell TO100 significantly increased its activity shortly after the rule change (rule 2-naive) ($p = 0.0103$, Kruskal-Wallis test, *post hoc* Dunn's multiple comparisons test), whereas cell TO23 increased activity only with the learning of the new task



(legend on next page)

rule (rule 2-learned) ($p = 0.0039$, Kruskal-Wallis test, *post hoc* Dunn's multiple comparisons test) (Figure 5D).

Neuronal Activity during the Delay Period Undergoes Diverse Changes with the Progression of Conflicting Trials

After reporting anatomical, physiological, and molecular diversity among the *in vivo* recorded and labeled mPFC cells with elevated spiking activity during the delay period of the working memory task, we sought to look further into the unidentified delay-elevated units from the tetrode and silicon probe recordings as well ($N = 30$ out of all recorded 123 cells in 16 rats). Consistently, we observed these cells were distributed across different cortical layers with similar proportions, and their firing rate adaptation to the rule change was non-uniform as calculated by the rule change scores (Figures 6A and 6B). Therefore, we did not observe a similar anatomical localization nor a systematic pattern of change in spiking activity during the delay period. In this paradigm, while one cue/reward arm contingency remain unchanged, the other cue type was leading to confusion. We tested the hypothesis that these diverse adaptations of the firing rate upon rule change might be specific for the trial subtypes. Therefore, we dissected the trials before and after the rule change in five groups (trials with a stable or changing cue, and non-conflicting correct, conflicting error, and conflicting correct trials), and tracked the changes of the recorded cells in these specific trial subtypes (Figure 6C, top). Interestingly, we found that the firing rate is not exclusively diversifying in the conflicting trials but also in the non-conflicting trials such that rule change induces a sudden unspecific excitation or inhibition onto the individual delay-elevated cells (Figure 6C, bottom).

In a previous study, we showed that prefrontal neurons in the mPFC signal for strategy switches rather than the task rules themselves (Malagon-Vina et al., 2018). Consistently, we found that prefrontal population activity during the memory delay undergoes trial-unspecific changes forming distant behavioral states. When each trial was represented as a population vector of neural activity during the delay period, the vectors tended to be temporally clustered in dimensionality reduction analysis, forming discrete and stimulus-unspecific state representations during cognitive flexibility (Figures 6D and 6E). We confirmed the marked changes between these neural state representations were due to the change in task rules but not the drift over time (Figure 6F).

As indicated earlier, conditional differences in firing rates among the correct cherry (right choices) and chocolate trials

(left choices) during the working memory task could be interpreted as a choice-selectivity feature. We hypothesized that if such differential activity of individual neurons can explicitly reflect the future choice, then the rule change should interrupt such differentiation due to the changing cue-reward arm contingency. Here, we report two mPFC neurons (TO20 and TO11), reflecting differential activity between stable and changing trials during rule 1 (Figures 6Gi and 6Gii, left panel). Upon rule change, while cell TO20 no longer exhibits differential activity as expected, cell TO11 maintains the differentiation of firing between the conflicting correct and non-conflicting correct trials when the animal receives distinct cues but chooses to go to the same reward arm (Figures 6Hi and 6Hii, right panel). At the population level, 6 out of 22 units that seemingly exhibited differential spiking activity prior to left and right choices during the delay period of rule 1 ("putative" choice selective cells) retained their differential pattern after the rule change. This finding suggests the integration of sensory response cannot be simply disambiguated from the choice selectivity feature of the individual mPFC cells (Figure 6H).

DISCUSSION

Here, we have demonstrated the diverse contributions of individual mPFC neurons to the network operations underlying working memory-guided decision-making and cognitive flexibility. We recorded the neuronal activity across all cortical layers from the rats performing a prefrontal-dependent cue-matching-to-place task (Lagler et al., 2016) followed by an unexpected rule change in a single behavioral session (Figure 1). What happens to the neuronal ensembles when the well-learned strategy requires an update? First, we have shown that individual units in the mPFC may undergo diverse adjustment in spiking activity upon rule change, cumulating in a complex firing rate reorganization that is balanced and well-distributed across the cortical layers of the mPFC at the population level. The task-episode modulation of the mPFC neurons sustains even after the task rules change and when the animals endeavor to resolve the conflict (Figures 2 and S1).

Despite the tremendous efforts to link a specific circuit with a certain behavior in systems neuroscience, we still do not know how many types of neuron exist and how distinct types of neuron contribute to cognition (Klausberger and Somogyi, 2008). The cerebral cortex comprises a variety of specialized cell types, which have been characterized by their spatial organization, dendritic arrangements, synaptic connectivity, electrophysiological

Figure 5. Activity of the Identified Delay-Tuned Neuron Reflects a Variety of Task-Relevant Processes and Exhibits a Diverse Molecular Expression Pattern

(A) Labeled delay-elevated and delay-suppressed principal neurons are distributed along the mediolateral and caudal-rostral axes in the prelimbic cortex. Red dots indicate the position of the identified cell body (D, dorsal; M, medial; and L, lateral).

(B) Autocorrelation histograms and the overall firing rate of each labeled cell.

(C) Raster plots of the identified delay-elevated and delay-suppressed neurons across all trials during rule 1, rule 2-naive and rule 2-learned.

(D) Normalized rate plot showing trial-by-trial deflections of the individual cells during the delay period across rule 1, rule 2-naive and rule 2-learned.

(E) Cue or choice selectivity, reflecting differential firing activities between correct chocolate and cherry trials was not shared across all labeled delay-tuned neurons. Asterisks indicate significance, calculated as described in Figure 3E, bottom. Dark lines, mean firing rate; shading, mean \pm SEM.

(F) The firing activity of individual delay-tuned neurons altered diversely upon rule change (black, non-conflicting trials; red, conflicting error trials; green, conflicting correct trials). Asterisks indicate significance ($*P_{TO24} = 0.0335$, $P_{TO31} = 0.1406$, $P_{TO20} = 0.6963$, $*P_{TO34} = 0.0337$, $P_{TO36} = 0.3128$, $P_{TO15} = 0.0053$, $P_{TO100} = 0.9642$, and $P_{TO23} = 0.3967$, Kruskal-Wallis test, *post hoc* Dunn's multiple comparisons test). Error bars denote \pm SEM.

Table 1. Physiological Parameters and Immunohistochemical Analyses of the Labeled Delay-Tuned Cells

Cell ID	Delay Elevated						Delay Suppressed	
	TO36	TO34	TO24	TO20	TO31	TO15	TO23	TO100
Layer	2	3	5	5	5	5	2	5
Overall firing rate (Hz)	3.44	1.67	1.58	1.77	2.86	2.21	2.84	5.43
Rule 1-delay $\Delta FR_{\text{choc,cher}}$	yes	yes	no	yes	no	no	no	no
Rule 2-delay $\Delta FR_{\text{choc,cher}}$	no	yes	no	no	no	yes	no	no
RCS rule 1 to naive	0.22249	-0.34134	-0.04442	0.049231	0.048907	0.243762	0.213187	0.208116
RCS rule 1 to learned	0.376147	0.034414	0.118487	-0.09658	-0.0791	-0.00254	0.422327	0.195335
RCS naive to learned	0.167691	0.371389	0.162055	-0.14512	-0.12752	-0.24615	0.229833	-0.01332
Immunoreactivity								
CTIP2	n+	n+	n+	n+	n+	u	n+	n+
BRN1	n+	n+	n+	n-	n+	u	n+	n+
WFS1	s+	s-	s+	s+	s-	u	d+	s+
SATB2	n+	n+	n-	n-	n+	u	n+	n+

Positive (+) or undetectable (-) immunoreactivity within the subcellular domain; s, soma; n, nucleus; d, dendrite; and u, unavailable or inconclusive. RCS, rule change score.

characteristics, and the presence of specific proteins and/or mRNAs. Cell-type-specific promoters are not abundant, and genetically defined subgroups often consist of several distinct types of neuron. In this study, we aimed to approach the phenomenon from a different perspective and focus on the pyramidal cells with distinct firing patterns during cognitive behavior and aimed to characterize those cells *post hoc* upon juxtacellular labeling technique. These are long single-cell juxtacellular recordings from the freely moving animals during cognitive task performance (34.18 ± 8.96 min; $N = 21$ cells).

Delay-period activity is thought to be central to working memory (Liu et al., 2014). Since the seminal works of Fuster, Goldman-Rakic, and colleagues dating back to the 1970s (Fuster and Alexander, 1971; Kojima and Goldman-Rakic, 1982), there have been numerous studies reporting a subset of prefrontal neurons with persistent activity during the so-called memory delay and their task-engaged properties such as rule encoding, accuracy, and goal representation with or without sensory integration widely varying across behavioral tasks in non-human primates. We aimed and managed to record and characterize these mPFC neurons showing significantly elevated or suppressed spiking activity during the delay period of the working memory paradigm in freely behaving rats. Contrary to primate studies, the robust persistent activity period does not span the entire delay period in rodents but rather shows bouts of activity that peak during different epochs of the delay (Runyan et al., 2017; Constantinidis et al., 2018). Our results from the identified neurons were in line with these reports (Figures 3, 4, and 5).

mPFC is topologically organized along the dorso-ventral axis in different sensory-motor-dependent tasks exhibiting a functional gradient and heterogeneity (Euston et al., 2012; Har-dung et al., 2017). In our electrophysiological recordings, the locations of cell bodies of the labeled (Figure 5A) and overall (Figure 6A) delay-tuned neurons were distributed along the dorso-ventral and medio-lateral axes of the prelimbic cortex; therefore, we did not observe a spatial clustering within the cortical organization.

Mixed selectivity of individual neurons brings high dimensionality, which may be necessary for achieving highly versatile and complex behavioral tasks (Rigotti et al., 2013). In freely moving animals, unlike head-restrained and motorically well-controlled recordings in monkeys, it is not easy to disambiguate in what exact cognitive computations these neurons play a part and neither do real-life operations in the cortex. Yet, a recent machine-learning study in freely moving rats provided evidence that firing related to various limb movements, poses, or spatial locations has little impact on single mPFC neurons; however, they are widely distributed at the ensemble level (Lindsay et al., 2018). We did not observe a discernible effect of grooming, rearing, or the direction of turning from cue to delay transition on delay-period activity (Figure S3). Nonetheless, we would like to emphasize that our findings do not exclude the possibility that delay-elevated activity may reflect a general attentive or task-engaged state. In fact, this may be in concordance with the largely sustained firing pattern during rule 2, when the delay-period activity is rendered irrelevant to choice. Taking this into account, we sought to investigate each recorded neuron separately in a bottom-up manner for the task-relevant processes their activity might be correlated with. Consistent with the previous reports, spiking activity of a subset of prefrontal neurons, but not all, during the delay signaled the upcoming choice (Figures 4, 5, and 6). If this differential spiking activity between the left and right choices during the memory delay is merely due to the neurons' choice-selective feature as previously reported, we posited that such differentiation should go away when the animals encounter a conflict in task rules and when the cue/reward contingency changes (Figure 6C). Surprisingly, a subset of neurons that separates between correct left and right choices during rule 1 kept the differential firing even after the rule change. Moreover, we observed a group of neurons that did not signal the upcoming choice during rule 1; however, they started to differentiate between correct conflicting and correct non-conflicting trials after the rule change. These findings provide evidence that neuronal activity during the delay period can hold multi-modal

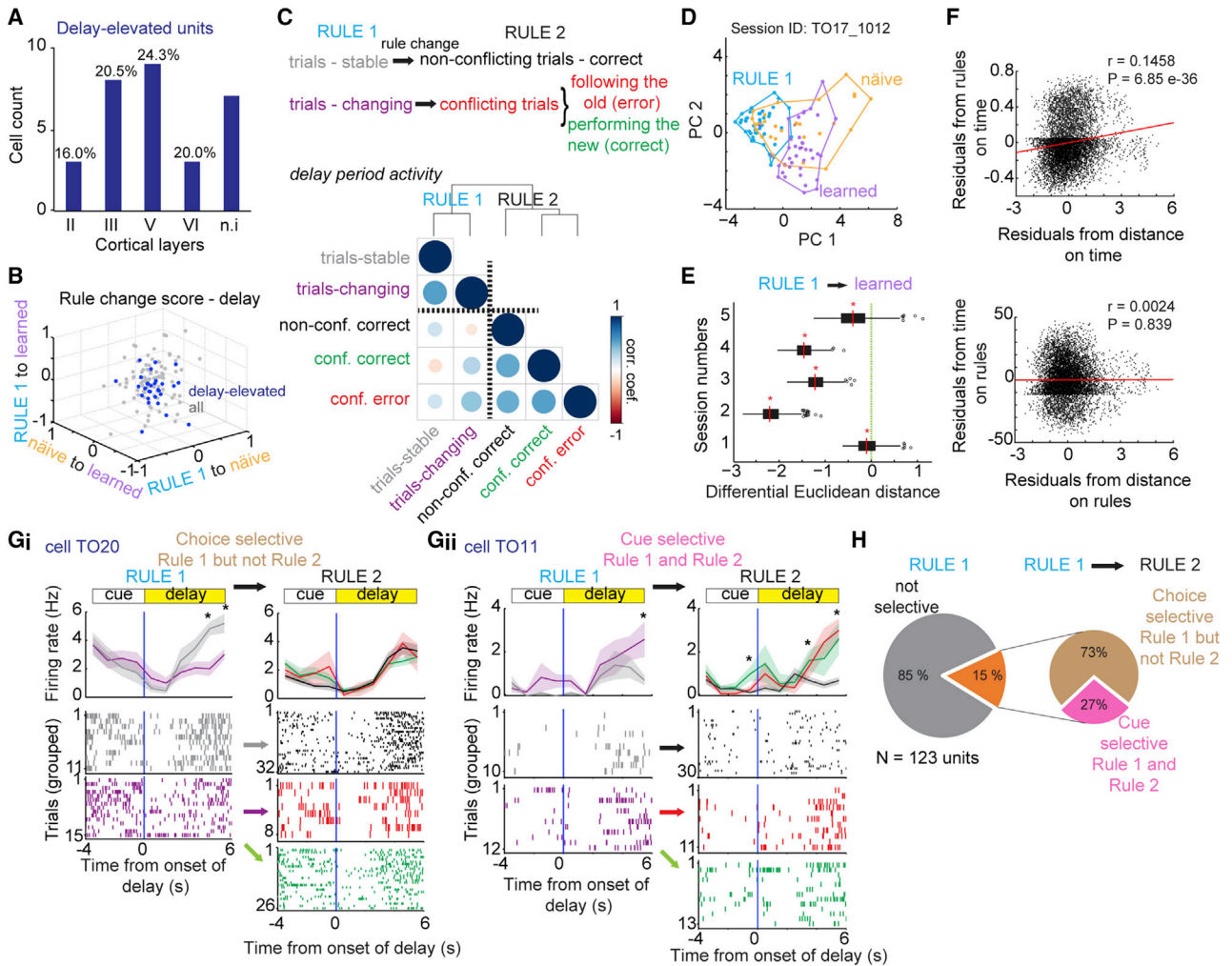


Figure 6. Trial Dynamics of the Activity during the Delay Period upon Rule Change

(A) Distribution of the delay-elevated units across cortical layers. The percentages above indicate the fraction of the delay-elevated cells in the corresponding layer ($N = 30$ units; $p = 0.6948$, Chi-square test).

(B) The firing activity of the delay-elevated cells underwent diverse changes across rule 2-naïve and rule 2-learned as indicated by rule change scores (RCSs) calculated only during the delay period (blue, delay-elevated units; gray, all units).

(C) Top: 5 prominent trial types of the behavioral paradigm before and after the rule change are summarized in the flow chart (gray, stable trials; magenta, changing trials; black, non-conflicting-correct trials; red, conflicting-error trials; and green, conflicting-correct trials). Bottom: pairwise Spearman rank correlation computed across all delay-elevated units and the coefficient matrix is reordered upon hierarchical clustering. Both the diameter of the circles and the intensity of the color are representative of R values. The horizontal and vertical dashed lines separate rule 1 from rule 2 to aid visualization.

(D) Projection of prefrontal multi-unit activity ($N = 32$ cells) during the delay period onto the first two principal components in a session. Each mark indicates a trial. (E) Normalized distribution of the differential distances (shuffles minus observed data) across 5 recording sessions in 3 rats. Euclidean distances were calculated from rule 1 to rule 2-learned for every multi-unit recording session. Zero (dotted green line) indicates the reference distance (observed data). Boxplots represent deviations of the distance obtained from shuffled data. For clarity, only stable/non-conflicting trials were used.

(F) Partial Pearson correlation plots of all possible Euclidean distances between the trials and rules (top), or the trials and time (number of trials in between) (bottom). This indicates that firing changes with rule switches but does not drift with time.

(G) Raster plots of the spiking activity of two delay-elevated units before and after the rule change, color coded corresponding to the five prominent trial types in Figure 6C. Persistent firing activity during the delay period in rule 1 is different between the cue (rule 1) for two recorded cells TO20 and TO11. (Gi, Gii, right panels). Choice/cue selectivity disappears with the rule change for TO20 but not for TO11. Asterisks indicate significance computed across conflicting correct and non-conflicting correct trials and is determined as described in Figure 3E, bottom; see STAR Methods for details. Dark lines, mean firing rate; shading, mean \pm SEM. (H) Quantification of the recorded cue- or choice-selective cells during working memory and flexibility behavior. Most of the neurons exhibiting differential firing activity between cherry (go right) and chocolate trials (go left) during the delay period of rule 1 did not exhibit this differential activity after the rule change when cue-reward contingency no longer matched with the old rule. (See also Figure S3.)

information that diversely transforms from case to case during adaptive behavior.

Flexible cognitive control is dependent on the activity of an intact mPFC (Ragozzino et al., 1999). The balance between stability and flexibility must be maintained for maximizing the output in goal-directed behavior. What happens to the persistent delay activity when the rats encounter a conflict and the current working memory strategy requires an update? Interestingly, the stereotypical firing patterns of individual delay-tuned cells remained largely similar; however, the cells diversely reacted to the change in task rules, exhibiting different rate adaptation either with the conflict abruptly and/or upon learning the new task rule (Figures 3F, 4E, 5C, and 6B). To find blueprints of the trials that induced changes in spiking activity upon a rule change, we further dissected the trial identities. Interestingly, we observed rule changes induced sudden unspecific changes onto the individual cells rather than with the direct encounter of specific conflicting trials. This might be an outcome of changing ensembles upon facing the conflict in the task rules, which potentially include an “aha” moment, as suggested in a previous study (Durstewitz et al., 2010).

Specific combinations of expressed genes have guided to profile cortical circuit organization in the developing (Gray et al., 2004) and adult brain (Zeisel et al., 2015). Our knowledge of cell-specific markers comes from *in situ* RNA hybridization data (Lein et al., 2007), technologies involving translating ribosome affinity purification (TRAP) in bacterial artificial chromosome (BAC) transgenic mice (Heiman et al., 2008), and microarray analyses combined with retrograde tracing (Arlotta et al., 2005). Notably, all these translational profiling options have been achieved at the mRNA level in mice, often determining genes whose expression is clustered in a specific cortical layer. Without the link between the molecular expression profile and function in cognition, our understanding of the nervous system will be restricted (Fishell and Heintz, 2013). Therefore, we sought to investigate if the identified delay-elevated neurons constituted a cell type in terms of molecular expression pattern. However, unlike inhibitory interneurons, reliable protein markers for selecting subtypes of pyramidal cells are very limited; thus, the diversity among these neurons remains underexplored. We tested the immunoreactivity of the available markers that labeled pyramidal neurons in the adult rat mPFC, with lesser layer dependency and co-localizations with each other (Figures 3H, 4G, and S2; Table 1). In spite of the low cell count of cells available for immunohistochemistry (N = 5 out of 6 neurons), we report that we did not find a shared molecular expression profile among these *in vivo* recorded and labeled delay-tuned cells in the working memory-guided decision-making task.

The mammalian mPFC is largely interconnected and it holds one of the most complex neuronal networks because it does not have a well-defined direct sensory input or motor output pathways. Dual perspectives on the persistent activity of single prefrontal neurons during working memory discuss whether the sustained activity of individual neurons or the rhythmicity constitutes the neural substrate of the working memory in monkeys (Lundqvist et al., 2018; Constantinidis et al., 2018). These are strong and valuable opinions; however, we would like to raise the concern that such substrates shall not be restricted to the

delay period however relevant this brief period appears to be to the psychological working memory definition. Our observation that rule change induces diverse and unselective adjustment of the neuronal activity while individual neurons' stereotypical firing patterns largely remain, stresses the importance of not assigning direct and temporally restricted substrates for working memory. The exact timing of the information retrieval and decision execution cannot be determined and often reflects the most plausible interpretation of the experimenters. Our interpretation of the brief bouts of activity with varying onset could indeed reflect some task relevance and, yet, dynamically alter its representation in its neuronal ensemble upon a rule change. Individual pyramidal cells with similar anatomical location may exhibit divergent responses during cognitive behavior.

In this study, we have brought together divergent domains to the neural pinning of the complex behavior. Collectively, our results demonstrate the anatomical, functional, and molecular diversity among the delay-tuned neurons during working memory-guided decision-making. Upon rule change, these cells undergo diverse changes in activity, supporting the complexity underlying prefrontal network operations for flexible cognitive control.

STAR METHODS

Detailed methods are provided in the online version of this paper and include the following:

- KEY RESOURCES TABLE
- LEAD CONTACT AND MATERIALS AVAILABILITY
- EXPERIMENTAL MODEL AND SUBJECT DETAILS
- METHOD DETAILS
 - Surgical procedure and implantation
 - Behavioral Paradigm
 - *In vivo* Recording and Juxtacellular Labeling in Behaving Rats
 - Multiple Single-Unit Recordings
 - Electrophysiological Data Analysis
 - Tissue Processing and Immunohistochemistry
 - Rule Change Score (RCS)
 - Determination of Delay-Tuning and Choice Selectivity
 - Correlation Circles, Hierarchical Clustering, Dendrogram
- QUANTIFICATION AND STATISTICAL ANALYSIS
- DATA AND CODE AVAILABILITY

SUPPLEMENTAL INFORMATION

Supplemental Information can be found online at <https://doi.org/10.1016/j.celrep.2019.12.102>.

ACKNOWLEDGMENTS

We would like to thank David Dupret, Gido van de Ven, and Vitor Lopes dos Santos for help with cell assembly analyses; Erzsebet Borok, Romana Hauer, and Elisabeth Dögl for excellent technical support; and Ece Sakalar, Thomas Forro, Abhilasha Joshi, Linda Katona, Tim Viney, and Peter Somogyi for their insightful discussions in the early stages of the data interpretation. This work was supported by grants P27610-B27 and W1205-BO9 of the Austrian Science Fund.

AUTHOR CONTRIBUTIONS

Conceptualization, A.T.O. and T.K.; Methodology, A.T.O., M.L., S.L., H.M.-V., B.L., and T.K.; Investigation, A.T.O., M.L., S.L., and T.K.; Writing – Original Draft, A.T.O. and T.K.; Writing – Review & Editing, A.T.O., M.L., S.L., H.M.-V., B.L., and T.K.; Funding Acquisition, T.K.; Supervision, M.L., B.L., and T.K.

DECLARATION OF INTERESTS

The authors declare no competing interests.

Received: January 25, 2019

Revised: June 28, 2019

Accepted: December 30, 2019

Published: February 4, 2020

REFERENCES

- Arlotta, P., Molyneaux, B.J., Chen, J., Inoue, J., Kominami, R., and Macklis, J.D. (2005). Neuronal subtype-specific genes that control corticospinal motor neuron development in vivo. *Neuron* 45, 207–221.
- Baddeley, A. (1992). Working memory. *Science* 255, 556–559.
- Bauer, R.H., and Fuster, J.M. (1976). Delayed-matching and delayed-response deficit from cooling dorsolateral prefrontal cortex in monkeys. *J. Comp. Physiol. Psychol.* 90, 293–302.
- Birrell, J.M., and Brown, V.J. (2000). Medial frontal cortex mediates perceptual attentional set shifting in the rat. *J. Neurosci.* 20, 4320–4324.
- Bolkan, S.S., Stujenske, J.M., Parnaudeau, S., Spellman, T.J., Rauffenbart, C., Abbas, A.I., Harris, A.Z., Gordon, J.A., and Kellendonk, C. (2017). Thalamic projections sustain prefrontal activity during working memory maintenance. *Nat. Neurosci.* 20, 987–996.
- Buckley, M.J., Mansouri, F.A., Hoda, H., Mahboubi, M., Browning, P.G.F., Kwok, S.C., Phillips, A., and Tanaka, K. (2009). Dissociable components of rule-guided behavior depend on distinct medial and prefrontal regions. *Science* 325, 52–58.
- Buzsáki, G. (2010). Neural syntax: cell assemblies, synapse ensembles, and readers. *Neuron* 68, 362–385.
- Constantinidis, C., Funahashi, S., Lee, D., Murray, J.D., Qi, X.-L., Wang, M., and Arnsten, A.F.T. (2018). Persistent spiking activity underlies working memory. *J. Neurosci.* 38, 7020–7028.
- Csicsvari, J., Hirase, H., Czurko, A., and Buzsáki, G. (1998). Reliability and state dependence of pyramidal cell-interneuron synapses in the hippocampus: an ensemble approach in the behaving rat. *Neuron* 21, 179–189.
- Del Arco, A., Park, J., Wood, J., Kim, Y., and Moghaddam, B. (2017). Adaptive encoding of outcome prediction by prefrontal cortex ensembles supports behavioral flexibility. *J. Neurosci.* 37, 8363–8373.
- Dias, R., Robbins, T.W., and Roberts, A.C. (1996). Dissociation in prefrontal cortex of affective and attentional shifts. *Nature* 380, 69–72.
- Durstewitz, D., Vitoz, N.M., Floresco, S.B., and Seamans, J.K. (2010). Abrupt transitions between prefrontal neural ensemble states accompany behavioral transitions during rule learning. *Neuron* 66, 438–448.
- Euston, D.R., Gruber, A.J., and McNaughton, B.L. (2012). The role of medial prefrontal cortex in memory and decision making. *Neuron* 76, 1057–1070.
- Fishell, G., and Heintz, N. (2013). The neuron identity problem: form meets function. *Neuron* 80, 602–612.
- Fujisawa, S., Amarasingham, A., Harrison, M.T., and Buzsáki, G. (2008). Behavior-dependent short-term assembly dynamics in the medial prefrontal cortex. *Nat. Neurosci.* 11, 823–833.
- Funahashi, S., Bruce, C.J., and Goldman-Rakic, P.S. (1993). Dorsolateral prefrontal lesions and oculomotor delayed-response performance: evidence for mnemonic “scotomas”. *J. Neurosci.* 13, 1479–1497.
- Fuster, J.M. (2015). *The Prefrontal Cortex, Fifth Edition* (Academic Press).
- Fuster, J.M., and Alexander, G.E. (1971). Neuron activity related to short-term memory. *Science* 173, 652–654.
- Gray, P.A., Fu, H., Luo, P., Zhao, Q., Yu, J., Ferrari, A., Tenzen, T., Yuk, D.-I., Tsung, E.F., Cai, Z., et al. (2004). Mouse brain organization revealed through direct genome-scale TF expression analysis. *Science* 306, 2255–2257.
- Haiss, F., Butovas, S., and Schwarz, C. (2010). A miniaturized chronic micro-electrode drive for awake behaving head restrained mice and rats. *J. Neurosci. Methods* 187, 67–72.
- Hardung, S., Epplé, R., Jäckel, Z., Eriksson, D., Uran, C., Senn, V., Gibor, L., Yizhar, O., and Diester, I. (2017). A functional gradient in the rodent prefrontal cortex supports behavioral inhibition. *Curr. Biol.* 27, 549–555.
- Harris, K.D., Henze, D.A., Csicsvari, J., Hirase, H., and Buzsáki, G. (2000). Accuracy of tetrode spike separation as determined by simultaneous intracellular and extracellular measurements. *J. Neurophysiol.* 84, 401–414.
- Hebb, D.O. (1949). *The Organization of Behavior: A Neuropsychological Theory* (Wiley).
- Heiman, M., Schaefer, A., Gong, S., Peterson, J.D., Day, M., Ramsey, K.E., Suárez-Fariñas, M., Schwarz, C., Stephan, D.A., Surmeier, D.J., et al. (2008). A translational profiling approach for the molecular characterization of CNS cell types. *Cell* 135, 738–748.
- Jacobsen, C.F. (1936). Studies of cerebral function in primates. I. The functions of the frontal association areas in monkeys. *Comp. Psych. Monogr.* 13, 1–60.
- Joel, D., Weiner, I., and Feldon, J. (1997). Electrolytic lesions of the medial prefrontal cortex in rats disrupt performance on an analog of the Wisconsin Card Sorting Test, but do not disrupt latent inhibition: implications for animal models of schizophrenia. *Behav. Brain Res.* 85, 187–201.
- Kamigaki, T., and Dan, Y. (2017). Delay activity of specific prefrontal interneuron subtypes modulates memory-guided behavior. *Nat. Neurosci.* 20, 854–863.
- Keays, D.A., Tian, G., Poirier, K., Huang, G.-J., Siebold, C., Cleak, J., Oliver, P.L., Fray, M., Harvey, R.J., Molnár, Z., et al. (2007). Mutations in α -tubulin cause abnormal neuronal migration in mice and lissencephaly in humans. *Cell* 128, 45–57.
- Kim, C.K., Ye, L., Jennings, J.H., Pichamoorthy, N., Tang, D.D., Yoo, A.W., Ramakrishnan, C., and Deisseroth, K. (2017). Molecular and circuit-dynamical identification of top-down neural mechanisms for restraint of reward seeking. *Cell* 170, 1013–1027.e14.
- Klausberger, T., and Somogyi, P. (2008). Neuronal diversity and temporal dynamics: the unity of hippocampal circuit operations. *Science* 321, 53–57.
- Klausberger, T., Magill, P.J., Márton, L.F., Roberts, J.D.B., Cobden, P.M., Buzsáki, G., and Somogyi, P. (2003). Brain-state- and cell-type-specific firing of hippocampal interneurons in vivo. *Nature* 421, 844–848.
- Kojima, S., and Goldman-Rakic, P.S. (1982). Delay-related activity of prefrontal neurons in rhesus monkeys performing delayed response. *Brain Res.* 248, 43–49.
- Kubota, K., and Niki, H. (1971). Prefrontal cortical unit activity and delayed alternation performance in monkeys. *J. Neurophysiol.* 34, 337–347.
- Lagler, M., Ozdemir, A.T., Lagoun, S., Malagon-Vina, H., Borhegyi, Z., Hauer, R., Jelem, A., and Klausberger, T. (2016). Divisions of identified parvalbumin-expressing basket cells during working memory-guided decision making. *Neuron* 91, 1390–1401.
- Lapray, D., Lasztoczi, B., Lagler, M., Viney, T.J., Katona, L., Valenti, O., Hartwich, K., Borhegyi, Z., Somogyi, P., and Klausberger, T. (2012). Behavior-dependent specialization of identified hippocampal interneurons. *Nat. Neurosci.* 15, 1265–1271.
- Lee, A.K., Manns, I.D., Sakmann, B., and Brecht, M. (2006). Whole-cell recordings in freely moving rats. *Neuron* 51, 399–407.
- Lein, E.S., Hawrylycz, M.J., Ao, N., Ayres, M., Bensinger, A., Bernard, A., Boe, A.F., Boguski, M.S., Brockway, K.S., Byrnes, E.J., et al. (2007). Genome-wide atlas of gene expression in the adult mouse brain. *Nature* 445, 168–176.
- Lindsay, A.J., Caracheo, B.F., Grewal, J.J.S., Leibovitz, D., and Seamans, J.K. (2018). How much does movement and location encoding impact prefrontal

- cortex activity? An algorithmic decoding approach in freely moving rats. *eNeuro* 5, ENEURO.0023-18.2018.
- Liu, D., Gu, X., Zhu, J., Zhang, X., Han, Z., Yan, W., Cheng, Q., Hao, J., Fan, H., Hou, R., et al. (2014). Medial prefrontal activity during delay period contributes to learning of a working memory task. *Science* 346, 458–463.
- Lodato, S., and Arlotta, P. (2015). Generating neuronal diversity in the mammalian cerebral cortex. *Annu. Rev. Cell Dev. Biol.* 31, 699–720.
- Lundqvist, M., Herman, P., and Miller, E.K. (2018). Working memory: Delay activity, yes! Persistent activity? Maybe not. *J. Neurosci.* 38, 7013–7019.
- Ma, L., Hyman, J.M., Durstewitz, D., Phillips, A.G., and Seamans, J.K. (2016). A quantitative analysis of context-dependent remapping of medial frontal cortex neurons and ensembles. *J. Neurosci.* 36, 8258–8272.
- Malagon-Vina, H., Ciocchi, S., Passecker, J., Dorffner, G., and Klausberger, T. (2018). Fluid network dynamics in the prefrontal cortex during multiple strategy switching. *Nat. Commun.* 9, 309.
- Matias, S., Lottem, E., Dugué, G.P., and Mainen, Z.F. (2017). Activity patterns of serotonin neurons underlying cognitive flexibility. *eLife* 6, e20552.
- McNamara, C.G., Tejero-Cantero, Á., Trouche, S., Campo-Urriza, N., and Dupret, D. (2014). Dopaminergic neurons promote hippocampal reactivation and spatial memory persistence. *Nat. Neurosci.* 17, 1658–1660.
- Miller, E.K. (2013). The “working” of working memory. *Dialogues Clin. Neurosci.* 15, 411–418.
- Miller, E.K., and Cohen, J.D. (2001). An integrative theory of prefrontal cortex function. *Annu. Rev. Neurosci.* 24, 167–202.
- Milner, B. (1963). Effects of different brain lesions on card sorting: The role of the frontal lobes. *Arch. Neurol.* 9, 90–100.
- Molnár, Z., and Cheung, A.F.P. (2006). Towards the classification of subpopulations of layer V pyramidal projection neurons. *Neurosci. Res.* 55, 105–115.
- Murray, A.J., Woloszynowska-Fraser, M.U., Ansel-Bollepalli, L., Cole, K.L.H., Foggetti, A., Crouch, B., Riedel, G., and Wulff, P. (2015). Parvalbumin-positive interneurons of the prefrontal cortex support working memory and cognitive flexibility. *Sci. Rep.* 5, 16778.
- Murugan, M., Jang, H.J., Park, M., Miller, E.M., Cox, J., Taliaferro, J.P., Parker, N.F., Bhave, V., Hur, H., Liang, Y., et al. (2017). Combined social and spatial coding in a descending projection from the prefrontal cortex. *Cell* 171, 1663–1677.e16.
- Nakayama, H., Ibañez-Tallon, I., and Heintz, N. (2018). Cell-Type-Specific Contributions of Medial Prefrontal Neurons to Flexible Behaviors. *J. Neurosci.* 38, 4490–4504.
- Narayanan, N.S., and Laubach, M. (2006). Top-down control of motor cortex ensembles by dorsomedial prefrontal cortex. *Neuron* 52, 921–931.
- Pinault, D. (1996). A novel single-cell staining procedure performed in vivo under electrophysiological control: morpho-functional features of juxtacellularly labeled thalamic cells and other central neurons with biocytin or Neurobiotin. *J. Neurosci. Methods* 65, 113–136.
- Ragozzino, M.E., Detrick, S., and Kesner, R.P. (1999). Involvement of the pre-limbic-infralimbic areas of the rodent prefrontal cortex in behavioral flexibility for place and response learning. *J. Neurosci.* 19, 4585–4594.
- Rich, E.L., and Shapiro, M. (2009). Rat prefrontal cortical neurons selectively code strategy switches. *J. Neurosci.* 29, 7208–7219.
- Rigotti, M., Barak, O., Warden, M.R., Wang, X.-J., Daw, N.D., Miller, E.K., and Fusi, S. (2013). The importance of mixed selectivity in complex cognitive tasks. *Nature* 497, 585–590.
- Rikhye, R.V., Gilra, A., and Halassa, M.M. (2018). Thalamic regulation of switching between cortical representations enables cognitive flexibility. *Nat. Neurosci.* 21, 1753–1763.
- Rossant, C., Kadir, S.N., Goodman, D.F.M., Schulman, J., Hunter, M.L.D., Saleem, A.B., Grosmark, A., Belluscio, M., Denfield, G.H., Ecker, A.S., et al. (2016). Spike sorting for large, dense electrode arrays. *Nat. Neurosci.* 19, 634–641.
- Rossi, M.A., Hayrapetyan, V.Y., Maimon, B., Mak, K., Je, H.S., and Yin, H.H. (2012). Prefrontal cortical mechanisms underlying delayed alternation in mice. *J. Neurophysiol.* 108, 1211–1222.
- Runyan, C.A., Piasini, E., Panzeri, S., and Harvey, C.D. (2017). Distinct time-scales of population coding across cortex. *Nature* 548, 92–96.
- Schmitt, L.I., Wimmer, R.D., Nakajima, M., Happ, M., Mofakham, S., and Halassa, M.M. (2017). Thalamic amplification of cortical connectivity sustains attentional control. *Nature* 545, 219–223.
- Szczepanski, S.M., and Knight, R.T. (2014). Insights into human behavior from lesions to the prefrontal cortex. *Neuron* 83, 1002–1018.
- Trouche, S., Koren, V., Doig, N.M., Ellender, T.J., El-Gaby, M., Lopes-Dos-Santos, V., Reeve, H.M., Perestenko, P.V., Garas, F.N., Magill, P.J., et al. (2019). A hippocampus-accumbens tripartite neuronal motif guides appetitive memory in space. *Cell* 176, 1393–1406.e16.
- van de Ven, G.M., Trouche, S., McNamara, C.G., Allen, K., and Dupret, D. (2016). Hippocampal offline reactivation consolidates recently formed cell assembly patterns during sharp wave-ripples. *Neuron* 92, 968–974.
- Zeisel, A., Muñoz-Manchado, A.B., Codeluppi, S., Lönnerberg, P., La Manno, G., Juréus, A., Marques, S., Munguba, H., He, L., Betsholtz, C., et al. (2015). Brain structure. Cell types in the mouse cortex and hippocampus revealed by single-cell RNA-seq. *Science* 347, 1138–1142.

STAR★METHODS

KEY RESOURCES TABLE

REAGENT or RESOURCE	SOURCE	IDENTIFIER
Antibodies		
Coup-TFI interacting protein 2 (CTIP2) [host Rb; Dil 1:1000]	Abcam	Cat# ab28448; RRID: AB_1140055
Wolfram syndrome-1 (WFS1) [host rb; Dil 1:1500]	Proteintech	Cat# 11558-1; RRID: AB_2216046
BRN1 [host gt; Dil 1:500]	Santa Cruz	Cat# sc6028, gift from Tibor Harkany, used in Keays et al. (2007)
SATB2 [host m; Dil 1:100]	Abcam	Cat# ab51502; RRID: AB_882455
Chemicals, Peptides, and Recombinant Proteins		
Neurobiotin Tracer	Vector Laboratories	Cat# SP-1120; RRID: AB_2313575
Critical Commercial Assays		
Vectastain ABC kit	Vector Laboratories	Cat# PK6100; RRID: AB_2336819
VECTASHIELD Antifade Mounting Medium	Vector Laboratories	Cat# H-1000; RRID: AB_2336789
Experimental Models: Organisms/Strains		
Long-Evans rats	Charles River Laboratories	https://www.criver.com/
Software and Algorithms		
MATLAB R2012b	Mathworks	https://www.mathworks.com/products/matlab.html
Prism 7	GraphPad	https://www.graphpad.com/
Spike2 7.11	Cambridge Electronic Design Limited (CED)	http://ced.co.uk/
Klustakwik	Harris et al., 2000	http://klustakwik.sourceforge.net/
klusta and KlustaViewA	Rossant et al., 2016	https://klusta.readthedocs.io/en/latest/
Zen	Zeiss	https://www.zeiss.co.uk/corporate/home.html
Imaris 9.2	BitPlane, Oxford Instruments	https://imaris.oxinst.com/
ImageJ 1.47v	ImageJ	https://imagej.nih.gov/ij/
Other		
Silicon Probe; Buzsaki64-H64_30mm	NeuroNexus	https://neuronexus.com/

LEAD CONTACT AND MATERIALS AVAILABILITY

Further information and requests for resources and reagents should be directed to and will be fulfilled by the Lead Contact, Thomas Klausberger (thomas.klausberger@meduniwien.ac.at). This study did not generate new unique reagents.

EXPERIMENTAL MODEL AND SUBJECT DETAILS

All animal procedures were performed under an approved license by the Austrian Ministry of Science and Medical University of Vienna, Austria. This study included sixteen male Long Evans rats (320 - 550 g, 2½ to 4 months old at the time of surgery) which were housed in a temperature- and humidity- controlled environment with a 12-hour light/dark cycle. Most recordings were performed between 12 and 6 p.m. (light cycle).

METHOD DETAILS

Surgical procedure and implantation

Implantation of the head-mounted set-up and stereotaxic surgeries were carried out as described in [Lagler et al. \(2016\)](#). Briefly, anesthesia was induced with 4% isoflurane (Forane®, AbbVie) in O₂ by inhalation and maintained on 1%–2% isoflurane throughout the surgery. After animals were mounted on the stereotaxic frame, 0.2 mL subcutaneous Xylocain® above the skull and 0.5ml/kg intraperitoneal Metacam® injections were carried out as analgesics. The skull was exposed under aseptic conditions. The body

temperature was maintained by using a heat pad and 2ml Ringer solution was given subcutaneously every two hours to prevent dehydration during the surgery. Upon recovery, rats were housed individually, and were food-deprived till they reach 85% of their initial body weight prior to behavioral training.

In this study, 15 rats underwent surgery for simultaneous glass electrode and tetrode recordings in prelimbic cortex (coordinates; AP +3.0 to 3.2 mm, ML +0.5 to 0.7 mm and AP +2.6 ML –1.2 mm, respectively). In 10 of these rats, a single tungsten wire was implanted into the dorsal CA1 hippocampus (coordinates; AP –3.2 mm, ML +2.3mm). Implantation for the juxtacellular recording was carried out as described in [Lapray et al. \(2012\)](#) for which we cemented (Refobacin®, Biomet) a cylindrical microdrive holder onto the skull approximately 6mm rostral to from the bregma. One rat was chronically implanted with a multi-shank silicon probe ([Key Resources Table](#)) spanning across the cortical layers in the prelimbic cortex (coordinates; AP +3.2mm ML 0.5 - 1.94 mm). In all rats, 4 stainless steel screws were fixed to the skull above the left parietal cortex and formed the basis for a headstage-connector. Two additional screws were fixed to the skull above the cerebellum and served as the ground and electrical reference for the recordings.

Behavioral Paradigm

Rats were trained to perform a delayed cue-matching-to-place task on an elevated Y-shaped maze. In this behavioral paradigm, rats randomly received a small amount of chocolate- or cherry-flavoured solution (18 μ l - both containing 15% sugar) that signaled the location of reward in one of the two reward arms of the maze (left or right, respectively). When correct, animals received a greater amount of the same type of stimulus in the reward arm (68 μ l). At the end of cue delivery, the animals' responses were delayed for six seconds with an automatic moveable door to probe working memory ([Lagler et al., 2016](#); [Fujisawa et al., 2008](#)). When rats reached 75% accuracy in task performance in > 3 consecutive days, juxtacellular glass electrode and tetrode recordings in prelimbic cortex (coordinates; AP +3 mm, ML +0.5 to 1 mm) were performed during this paradigm. While the rats were performing this well-learned task with high accuracy during a recording session, we introduced an abrupt rule change after which they could receive the reward only in one of the reward locations regardless of the cue type (Rule 2-naive). Although rats received randomized cue in the start arm as before, reward was only available at one of the two reward arms ever after. We set a threshold for starting to learn the task rule (Rule 2-learned) where rats switched the strategy in 5 conflicting trials consecutively excluding non-conflicting trials. None of the rats were habituated or trained to the rule change. In the recording sessions where the rat had exposed a similar rule change earlier (8 out of 24 sessions), there were no difference in behavioral parameters observed in terms of the number of errors made till learning ($p = 0.22763$, $r = -0.2558$, Spearman's correlation) or the number of trial counts till learning ($p = 0.1284$, $r = -0.3192$; Spearman's correlation). The flavour-side arm contingency varied across different rats and to prevent odour-guided strategies, both reward arms contained odour distractors (a large amount of mixed cherry and chocolate solution unreachable for the rats). Upon juxtacellular recording and labeling of single neurons ([Pinault, 1996](#)), rats were deeply anaesthetised and perfusion-fixed.

In vivo Recording and Juxtacellular Labeling in Behaving Rats

Extracellular single cell recording and labeling with neuronal tracer Neurobiotin reveal the identity of the *in vivo* recorded cells. At the end of the behavioral training, anesthesia was induced by isoflurane (Forane®, AbbVie) with airflow prior to opening a cranial window above the PFC. Exposed dura mater was treated with Mitomycin (0.1 mg/ml Sigma) to decelerate growth tissue formation. The brain surface was covered with a thin layer of paraffin wax and silicon (Kwik-Cast, World Precision Instruments) until the next day for glass electrode recordings. On the recording days, rats were briefly anesthetized with isoflurane, paraffin wax was removed, and glass electrode filled with 3% neurobiotin ([Key Resources Table](#)) in 0.5M NaCl was lowered to the cerebral surface. Subsequently, a miniaturized pre-amplifier and a protective cap carrying two LED arrays were attached to the chronically implanted head stage. Rats were left to recover in a chamber over 2 hours and using a piezoelectric motor (Kleindiek Nanotechnik) the glass electrode was remotely advanced to the target area ([Lee et al., 2006](#); [Lagler et al., 2016](#)). During the task performance while in Rule 1, the glass electrode was further lowered to approach a delay-tuned neuron. Because the spike trains were converted in an audio signal, ramping or dampening sound of spike output during the transition from cue delivery to delay were indicative of the target neuron. Following the successful recording of a delay-tuned neuron during Rule 1 over 15 trials, the rule change was introduced abruptly. When the rats achieved to pass the set behavioral threshold (5 consecutive conflicting correct choices), the glass electrode was further advanced to its juxta position and an attempt was made to the label the target cell with neurobiotin as described in [Pinault \(1996\)](#). If the labeling attempt was considered successful, the glass electrode was slowly retracted, the animal was deeply anesthetized and perfusion-fixed after 45 minutes to 2 hours to allow for neurobiotin to be transported in the neuron. If no labeling attempt were made or the labeling attempt was deemed unsuccessful, the recording session was terminated, and the brain surface was covered with paraffin wax and silicon as described before. This process was repeated on a different recording day until the animal was perfused. For the next recording session, the alternative arm was rewarded in Rule 2. Overall 9 cells were recorded and labeled during the first rule change ever experienced by the animal, 6 were labeled after the second rule change experienced by the animal. No differences were observed between these recordings. All recordings were carried out in a dimmed room and the animal behavior was monitored with an infrared camera, in addition to the camera used for position tracking. Maze was automatically controlled with a built-in (Data Acquisition Toolbox) and custom-written software in MATLAB (MathWorks). Neural signals from the glass electrode recordings were amplified 1000 times (DPA-2FS NPI Electronic GmbH) and filtered in two different frequency ranges (LFP;

0.3–300 Hz, action potentials; 0.8–5 kHz) and digitized at 20kHz (Power 1401 mkII A/D board; Cambridge Electronic Design). Line frequency noise (50 Hz) was removed using HumBug (Quest Scientific Instruments).

Multiple Single-Unit Recordings

Multiple single cell recordings with chronically implanted tetrodes and silicon probe help identify stereotyped activity patterns at the population level in the mPFC. Prior to implantation, 1 or 2 tungsten wire tetrodes (13 μm thick, California Fine Wire) were gold plated (100–500 k Ω) and mounted on a movable custom-made microdrive (Haiss et al., 2010). The signals from the tetrode recordings were amplified 1000 times and filtered between 0.3 and 5 kHz (EXT-16DX, NPI Electronic GmbH), and digitized at 20kHz. In one rat, we recorded the neural activity across all cortical layers simultaneously with an eight-shank silicon probe (Key Resources Table) in the mPFC. This probe was mounted on a custom-made moveable drive, and across recording days were slightly advanced in prelimbic cortex. Signals from the silicon probe recordings were amplified using a miniaturized headstage (HS-132A, 2 \times 32 channels, Axona Ltd). Output signals were amplified 1000 times via a 64-channel amplifier and then digitized at a sampling rate of 24 kHz, using an analog-to-digital converter computer card (Axona Ltd.). Single-units were detected offline by thresholding the digitally filtered signal at 0.8–5 kHz frequencies.

Electrophysiological Data Analysis

For tetrode recordings, spikes putatively belonging to the same neuron were isolated as described in Csicsvari et al. (1998) and clustered using KlustaKwik software (Harris et al., 2000). For silicon probe recordings, spike detection, feature extraction and automatic clustering were achieved using open source klusta and KlustaViewa software (Rossant et al., 2016). Each cluster included in this study had clear refractory period in its autocorrelation histogram, exhibited clear and stable spike waveform, and lacked the refractory period in its cross-correlation histogram with the other simultaneously recorded clusters (McNamara et al., 2014). All data analyses after spike sorting were performed using Spike2 (Cambridge Electronic Design) and built-in or custom-written software in MATLAB (MathWorks). Firing rates (spikes/s) were computed across sequential task epochs. We split each trial into 24 time-windows spanning across all epochs (3 during pause, 4 during cue, 6 during delay, 3 during run, 4 during reward, 1 during post-reward/no reward episode, 3 during return) as described in Figure 1B.

Tissue Processing and Immunohistochemistry

Rats were deeply anesthetized with urethane (2.5 g/kg body weight i.p.) and transcardially perfused with saline followed by 20 minutes of fixative (4% paraformaldehyde w/v, 15% v/v saturated picric acid, 0.05% glutaraldehyde in 0.1M phosphate buffer (PB) at pH 7.2). Some brains were post-fixed for 2 hours at 4°C in glutaraldehyde-free fixative. After fixation, brains were washed with 0.1M PB, coronal sections (50–60 μm) were cut using a vibratome (Leica VT 1000S, Leica Microsystems) and stored in 0.1M PB with 0.05% sodium azide at 4°C for further processing. To visualize labeled cells, selected sections were permeabilized with either rapid 3x freeze-thaw over the liquid nitrogen (upon cryo-protection with 20% sucrose in 0.1M PB) or with Tris-buffered saline (TBS) containing 0.3% Triton X-1000 (TBST). Then, sections were incubated with Streptavidin-conjugated fluorophores (1:1000 Alexa Fluor® 488 (Invitrogen) or 1:100 AMCA (Jackson ImmunoResearch Laboratories Inc.) in TBS. To visualize proteins in the selected cells, the permeabilized sections were first blocked with 20% normal horse serum in TBST for 40 minutes at room temperature, then incubated with TBS containing primary antibody (Key Resources Table) for 2 to 3 days at 4°C. Afterward, sections were incubated with secondary antibodies conjugated to Alexa Fluor® 488 (Invitrogen), Alexa Fluor® 405 (Abcam) and to AMCA, Cy3 or Cy5 (Jackson ImmunoResearch Laboratories Inc.) in TBS overnight at 4°C. Sections were thoroughly washed and mounted on glass slides in Vectashield® (Vector Laboratories Inc.) to be visualized under wide-field epifluorescence microscope (Olympus BX61) or confocal microscopes (Leica SP5 and Zeiss LSM880). Immunopositivity was accepted only if subcellular locations of target proteins, pattern and strength of the signal were comparable to non-labeled cells in the same section. If subcellular compartment lacked the detectable immunoreactivity, we could subsequently test other primary antibodies on the same sections. Counting of the cells with detected immunolabelling was performed using Imaris 9.2 and ImageJ 1.47v. Prior to reconstruction with NeuroLucida® (MBF Bioscience) (Olympus BX61 using 100x oil immersion objective (NA 1.4)), sections were processed with horseradish peroxidase based diaminobenzidine (DAB) reactions to reveal Neurobiotin signal as described in Klausberger et al. (2003).

Rule Change Score (RCS)

Each unit's mean firing rate (Hz) during Rule 1 and Rule 2-learned were calculated. The rule change score was computed as follows:

$$\text{Rule Change Score (RCS)} = \frac{\text{rate}(\text{Rule 2_learned}) - \text{rate}(\text{Rule 1})}{\text{rate}(\text{Rule 2_learned}) + \text{rate}(\text{Rule 1})}$$

where positive RCS value indicated an increase in firing rate with learning the new rule whereas negative RCS value indicated a decrement in the firing rate. Then, the trials were repeatedly shuffled for 1000 times and RCS was re-calculated each time to generate a surrogate score vector. Based on this vector's distribution, the lower bound of 2.5% and upper bound of 97.5% confidence interval were determined. If the actual RCS did not fall between the boundaries, the cell was accepted to significantly tune its firing rate with the learning of the new rule. We computed RCS across 'Rule 1 to naive', and 'naive to learned' using the same formula for a more detailed overview of the rate changes during cognitive flexibility.

Determination of Delay-Tuning and Choice Selectivity

Assessment of delay tuning property (delay-elevated or delay-suppressed) of single cells was carried out in few steps. As described earlier (see Figure 1B), we first calculated each unit's actual firing rate (Hz) in 1 s time windows (24/trial) and averaged across correct trials during Rule 1. Then, we randomly shuffled the time windows within a trial for every trial, calculating a surrogate firing rate. We repeated this procedure 10000 times, through which we obtained the p values of episodic firing modulation by comparing the actual firing rate to the surrogate distribution of rates (Lagler et al., 2016). For multiple comparisons, significance limits were corrected using false discovery rate (FDR) method. Cells with significant delay-episode modulation were selected and tested for their ramping or dampening activity from the cue. If the cell's firing rate during the delay-episode was greater than cell's overall firing rate (~24 s) and its peak firing bin fell in delay episode within cue-to-delay time windows (10 s), the cell was deemed delay-elevated. Contrarily, if the cell's firing rate during the delay-episode was less than cell's overall firing rate (~24 s) and its trough firing fell in delay episode within cue-to-delay time windows (10 s), we the cell was deemed delay-suppressed.

Identifying significant conditional differences in firing rate regarding choice- or cue-selectivity was determined with a permutation test with two conditions as described in Fujisawa et al. (2008) and Lagler et al. (2016). In brief, the difference of PSTHs of correct cherry trials and chocolate trials within cue-to-delay time windows (10 s) were computed. For the shuffling procedure, cherry/chocolate trial identities were randomized and permuted as described above through which we obtained the p values of selective bins (1 s) by comparing the actual difference with the surrogate distribution of rate differences. For multiple comparison, significance limits were corrected using false discovery rate (FDR) method. Subsequently, one sample Wilcoxon test was applied to avoid aberrant significance rising due to very low spiking activity in a given time bin.

Correlation Circles, Hierarchical Clustering, Dendrogram

Pairwise Spearman's correlation was computed on z-normalized delay firing activity of each cell, averaged for each trial type (stable trials, changing trials, conflicting correct trials, non-conflicting correct trials and conflicting error trials) using R. The correlation coefficients were plotted using the "corrplot" package, sorted using "hclust" function and dendrogram was generated using an in-built "heatmap" function.

QUANTIFICATION AND STATISTICAL ANALYSIS

Standard functions and custom-written scripts in MATLAB and Prism were used to perform analyses. Error bars in the figures represent standard error of the mean and number of experiments is indicated by n in figure legends. If not stated otherwise the alpha is 0.05. Statistical testing was two-tailed and the datasets were tested for normal distribution before applying parametric tests or non-parametric tests.

DATA AND CODE AVAILABILITY

The data and code that support the findings of this study are available from the corresponding authors upon request.